observations suggest that blood Vpr could induce various clinical symptoms, but it remained unclear whether blood Vpr is biologically active.

Long interspersed element-1 (LINE-1, L1) and Alu are major endogenous retroelements, accounting for ~17 and ~10% of the human genome, respectively [8,9]. As an autonomous retroelement, L1 can retrotranspose not only itself but also other retroelements, such as Alu and SVA (short interspersed element-variable number tandem repeat-Alu, SINE-VNTR-Alu). Intriguingly, a single human cell contains more than 5×10^5 copies of L1, 80–100 of which are competent for retrotransposition (L1-RTP) [10]. During early embryogenesis, L1-RTP incidentally disrupts gene structures, leading to the development of inborn errors [11,12]. Of note, approximately 100 types of inheritable diseases have been identified as sporadic cases caused by mutagenic RTP of L1 or Alu [12]. Although most studies of L1-RTP have focused on early embryogenesis [13-16], recent lines of evidence suggest that L1-RTP is also induced in somatic cells [17-20]. In tumors of epithelial-cell origins and hepatomas, *de novo* L1 insertions were detected in the vicinity of tumor suppressor genes, suggesting that L1-RTP is actively involved in carcinogenesis [21,22]. Because L1-RTP alters cellular properties by causing various genetic alternations, including gene deletions [23,24], DNA damage [25], apoptosis [26] and immune responses [27], deregulation of L1-RTP in somatic cells likely functions as a trigger of various diseases.

Here we present evidence that Vpr is active for induction of L1-RTP, and further demonstrate that 6 of 15 blood samples from HIV-1 patients were positive for Vpr-induced L1-RTP. Interestingly, rVpr reproducibly induced L1-RTP in various organs, including the kidney, when administered to mice that harbored human L1 as a transgene (hL1-Tg mice) [28,29]. Clinically, HIV-1-associated nephropathy (HIVAN), which is mainly observed among African-Americans [30], is an end-stage renal deficiency that is found without apparent correlation with the viral load [31,32]. In view of reports that Vpr is a candidate molecule responsible for HIVAN [33,34], we propose that monitoring blood levels of Vpr is important for determining its involvement in the pathogenesis of HIVAN.

Results

rVpr induces L1-RTP

We initially performed a colony formation assay using purified rVpr and pCEP4/L1*mneo*I/ColE1 (pL1-Neo^R) (Figure 1A and B) [28,35-37]. When HuH-7 human hepatoma cells were treated with rVpr, L1-RTP occurred in approximately 50 of 10^5 cells (Figure 1C, $P < 0.02$). rVpr caused no apparent cytotoxicity (Additional file 1: Figure S1). The activity of rVpr was also confirmed by a PCR-based assay using pEF06R [37,38], in which the signal intensity of the 140 bp band, which corresponds to a product of L1-RTP, was increased by treatment with rVpr (Figure 1B, lower panel for the rationale of the PCR-based assay and 1D, lane 2). A quantitative PCR (qPCR) analysis was also carried out using a TaqMan probe designed to detect a junction point of two exons of the *EGFP* gene (Figure 1B, bottom; see also Additional file 2: Figure S2 for standard qPCR curves). Data revealed that rVpr significantly increased the frequency of L1-RTP (Figure 1E, $P < 0.05$). Notably, rVpr-induced L1-RTP was completely blocked by 8D1 and C217, monoclonal antibodies (mAbs) against Vpr (Figure 1D, lanes 5 and 6) [4], but not by an irrelevant mAb against a spike protein of severe acute respiratory syndrome coronavirus (Figure 1D, lane 4, SARS). Vpr-induced L1-RTP was also observed in HEK293T cells, in which the activity of ~1 ng/mL rVpr was detected (Figure 1F, lanes 10–12; Additional file 3: Figure S3).

Taking advantage of the high sensitivity of the PCR-based assay performed using HEK293T cells, we explored the activity of L1-RTP in blood samples from HIV-1-positive patients. Among 15 samples analyzed by a PCR assay, 6 were positive for L1-RTP induction (Figure 2A, upper panel; patients' clinical information is summarized in Additional file 4: Table S1). Notably, L1-RTP activity was selectively blocked by 8D1, indicating that the L1-RTP activity in HIV-1 patients is attributable to Vpr (Figure 2B and C). Interestingly, Vpr-induced L1-RTP was detected in patients with low HIV-1 titres (Figure 2D and Additional file 4: Table S1). To confirm this, we carried out immunoprecipitation followed by Western blot analysis (IP-WB analysis), and successfully detected Vpr in one of two blood samples that were positive for L1-RTP (no. 15; Additional file 5: Figure S4, arrowhead). Estimated concentration of the blood Vpr, when compared to the signals of standard rVpr, would be approximately 5 ng/mL (Additional file 5: Figure S4). In contrast, we could not detect Vpr in another sample (no. 1).

rVpr induces L1-RTP *in vivo*

To determine the effects of rVpr *in vivo*, we next investigated L1-RTP after administration of rVpr to hL1-Tg mice (Figure 1B, solid line). As shown in Figure 3A, L1-RTP was detected in organs including the lymph nodes, liver, thymus and spleen upon intraperitoneal administration of ~200 ng of rVpr three times every 2 days (Additional file 6: Table S2). Interestingly, the qPCR analysis detected L1-RTP in the kidney after six intravenous administrations of 10 ng of rVpr (Figure 3B). To demonstrate that rVpr-induced L1-RTP was dependent on the reverse transcriptase activity of ORF2 [9], we first carried out *in vitro* experiments to examine whether rVpr-induced L1-RTP was blocked by nucleotide analogue

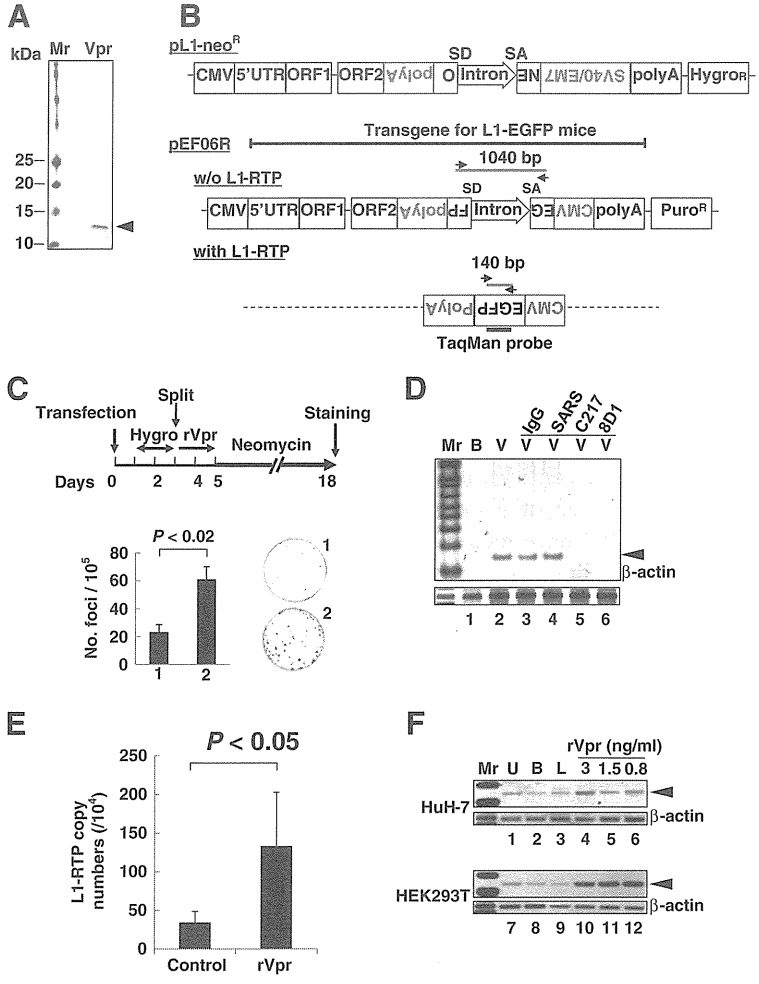

Figure 1 rVpr induces L1-RTP. A. rVpr was purified by two-step column chromatography using a glutathione-bead and an affinity column with 8D1. Purified protein was stained with Coomassie brilliant blue. Mr, molecular weight marker. **B**. Schematics of constructs used in the current study (see details in Methods). The PCR-based assay detects a 140 bp band that was amplified upon induction of L1-RTP (with L1-RTP), whereas it detects a 1040 bp band without L1-RTP (w/o L1-RTP). Arrows indicate primers for the PCR-based assay. SD and SA indicate splicing donor and splicing acceptor, respectively. The position of the TaqMan probe was also depicted. **C**. Colony formation assay of rVpr-induced L1-RTP. The experimental protocol and results are shown. HuH-7 cells were treated with buffer (plate no. 1) or rVpr (plate no. 2) are also shown. Obtained colonies were stained (right panels). **D**. Inhibition of rVpr-induced L1-RTP by mAbs against Vpr. 8D1 or C217 were used (lanes 5 and 6). As control, mouse IgG (lane 3) or a SARS mAb (lane 4) were included. B, buffer; V, rVpr. Arrowhead indicates the 140 bp band. Mr, molecular weight marker. **E**. Results of the qPCR analysis of rVpr-induced L1-RTP. Approximately 10 ng/mL of rVpr was used, and L1-RTP was measured by the qPCR. **F**. Activity of low dose of rVpr on HEK293T cells. Results of HuH-7 cells and HEK293T cells were shown. U, untreated; B, buffer; L, LPS (10 ng/mL).

inhibitors of reverse transcriptase (RTIs) [39,40]. As shown in Figure 3C, stavudine (d4T) and tenofovir inhibited the rVpr activity for L1-RTP induction (lanes 3 and 4), but lamivudine (3TC) and azidothymidine (AZT) did not (lanes 1 and 2). The inhibitory effects of d4T on rVpr-induced L1-RTP were potent, and the compound could effectively block the induction of L1-RTP at a concentration of 5 μM (Additional file 7: Figure S5). We next investigated the effects of 2′,3′-didehydro-3′-deoxy-4′-ethynylthymidine (4′-Ed4T), a stavudine analogue with more specific activity as an RTI and fewer side effects [41]. As shown in Figure 3D, 50 μmoles of 4′-Ed4T, when administered intraperitoneally 2 h before intravenous administration of 250 ng of rVpr, efficiently attenuated L1-RTP (compare lanes 2 and 3). qPCR analysis also clearly showed the inhibitory effects of 4′-Ed4T (Figure 3E).

By immunohistochemical analysis using α-GFP, we successfully detected cells positive for the induction of L1-RTP after a single injection of 2 μg or 250 ng of Vpr (Figure 4A). Intriguingly, L1-RTP occurred at a frequency of several cells per 10^4 cells after six administrations of 10 ng of rVpr (Figure 4B, $P < 0.05$). Co-administration

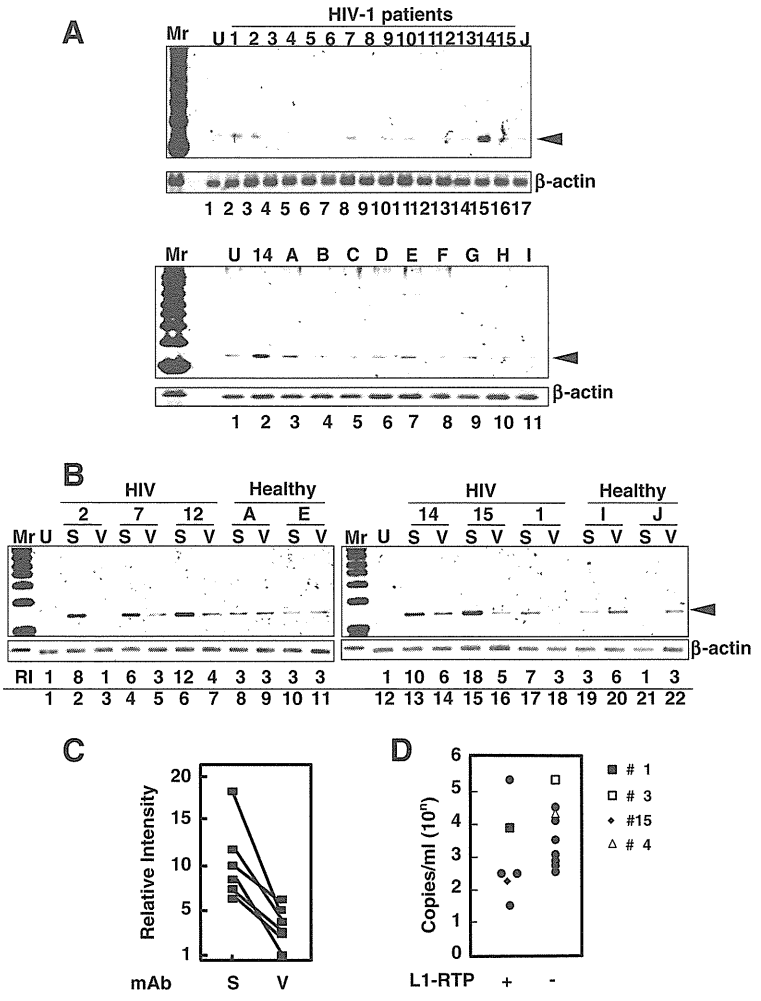

Figure 2 Detection of Vpr-induced L1-RTP in blood samples of HIV-1-positive patients. A. Upper panel. Activity for the induction of L1-RTP in the blood of HIV-1-positive patients. Results of the PCR-based assay were shown. Lower panel. As a control, samples of nine healthy volunteers were included (A–I). U, Untreated. **B**. A mAb against Vpr blocked the activity in serum samples. Serum sample of 300 μL was treated with ~500 ng 8D1 (V) or SARS-mAb (S). Serum samples from healthy volunteers were also included (Healthy, A, E, I and J). RI, relative intensity. **C**. Effects of 8D1 on the activity of L1-RTP. RI shown in Figure 2B was plotted and compared. S, treatment with a mAb to SARS; V, 8D1. 8D1 considerably attenuated the L1-RTP-inducing activity in the patients' blood. **D**. Detection of Vpr-induced L1-RTP in patients with lower viral titres with (+) or without (–) L1-RTP activity. According to the presence of the activity of L1-RTP in blood, patients were separated into two groups. Then, viral loads of each patient were plotted. Blood samples of two patients of each group were subjected to the IP-WB analysis. Vpr was detected in one patient (no. 15, ◆) (Additional file 5: Figure S4). Vpr was not detected in the sample of patient no. 1 (■), who was positive for L1-RTP. Other two patients were negative for both the activity of L1-RTP and Vpr (patient no. 3 and 4, □ and △).

of 4′-Ed4T significantly blocked L1-RTP induced by repetitive injection of 250 ng of rVpr (Figure 4C, column 3). Consistent with the results obtained by hematoxylin-eosin (H/E) and α-GFP staining, dual staining for α-aquaporin-1 or α-phalloidin, which are markers of proximal renal tubular cells [42-44], detected rVpr-induced L1-RTP in renal tubular epithelial cells (RTECs) (Figure 4D).

We also investigated the methylation status of CpG in the L1-5′UTR in the rVpr-treated kidney. Analysis by the COBRA method [45], a method of quantifying CpG methylation, detected no apparent changes in the methylation status of CpG before or after six administrations of 10 ng of rVpr (Additional file 8: Figure S6).

rVpr-induced L1-RTP depends on an AhR-p38-C/EBP-β cellular cascade

Previously, we reported that various environmental compounds induced L1-RTP in a manner dependent on the aryl hydrocarbon receptor (AhR), which has been shown to associate with other cellular molecules via an LxxLL motif in the counterpart molecule (amino acids denoted by single letters) [46]. Interestingly, Vpr contains

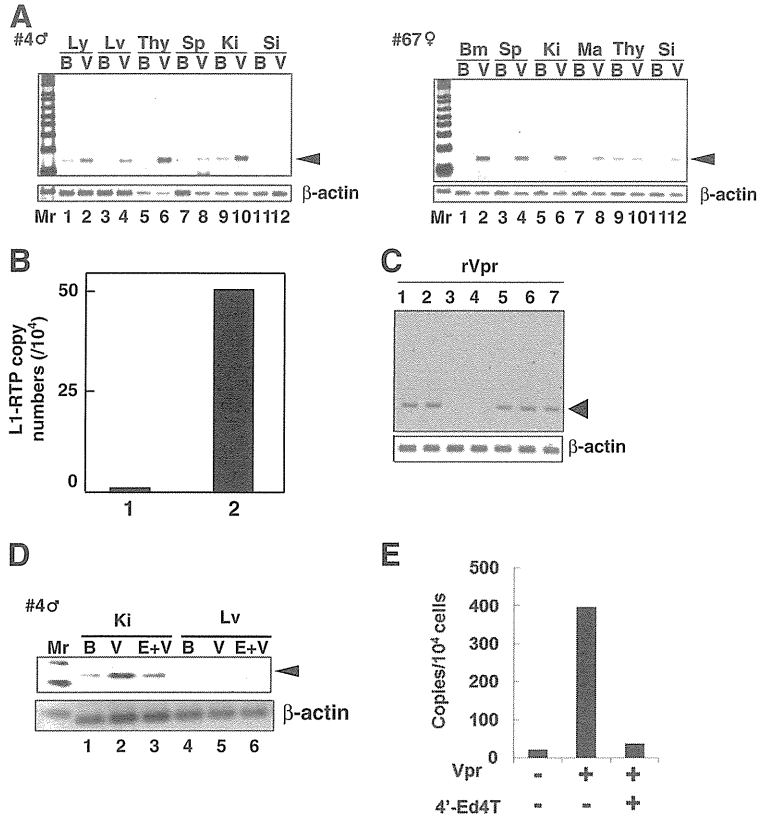

Figure 3 L1-RTP induction by rVpr *in vivo*. A. Induction of L1-RTP after intraperitoneal injection of rVpr. rVpr (200 ng; three injections every 2 days) was administered intraperitoneally into two strains of hL1-Tg mice (#4 and 67). On day 2 after the last injection, DNA was extracted from each organ and subjected to the PCR-based assay. Ly, lymph node; Lv, liver; Thy, thymus; Sp, spleen; Ki, kidney; Si, small intestine; Bm, bone marrow; Ma, mammary gland; B, buffer; V, rVpr. Arrowhead indicates L1-RTP. Mr, molecular weight marker. **B**. Effects low dose of rVpr. hL1-Tg mice (#4) were injected six-times with buffer (lane 1) or 10 ng rVpr (lane 2), and DNA extracted from kidney was subjected to the qPCR analysis. **C**. RTIs blocked rVpr-induced L1-RTP. Effects of RTIs (25 μM each) on rVpr-induced L1-RTP was examined. Lane 1, 10 ng/mL rVpr + lamivudine; lane 2, rVpr + AZT; lane 3, rVpr + d4T; lane 4, rVpr + tenofovir; lane 5, rVpr + nevirapine; lane 6, rVpr + efavirenz, lane 7, rVpr + saquinavir. **D**. RTIs inhibited rVpr-induced L1-RTP *in vivo*. Two hours before intravenous administration of 250 ng rVpr, 50 μmoles of 4′-Ed4T was injected intraperitoneally. Lanes 1 and 4, buffer (B); lanes 2 and 5, rVpr (V); lanes 3 and 6, rVpr + 4′-Ed4T (E); Ki, kidney; Lv, liver. **E**. Results of qPCR assay. Similar experiments with Figure 2D were done, and L1-RTP was measured by the qPCR.

an LQQLL motif at amino acids 64–68 that functions as a sequence motif for binding to host cellular proteins, including p300/histone acetyl transferase [47]. Based on these observations, we hypothesized that AhR functions as a cellular factor responsible for rVpr-induced L1-RTP. To prove this, we first assessed the effects of 3′-methoxy-4′-nitroflavone (MNF), an AhR inhibitor [48], and observed that 10 μM MNF completely blocked rVpr-induced L1-RTP (Additional file 9: Figure S7). Moreover, down-regulation of endogenous AhR expression by *AhR* siRNA was accompanied by reduced rVpr-induced L1-RTP (see Figure 5A, lane 4, and 5B for a representative result from experiments using two different *AhR* siRNAs; see also Additional file 10: Figure S8A and B for data obtained using another *AhR* siRNA). By contrast, down-regulation of ARNT1 by siRNA (Figure 5C) did not attenuate L1-RTP (Figure 5D, lane 9 and Additional file 10: Figure S8D, lane 9). AhR and ARNT1 form a heterodimer (AHR complex) and are involved in the induction of *CYP1A1* mRNA expression in response to environmental pollutants [49]. Both *AhR* and *ARNT1* siRNAs blocked the induction of *CYP1A1* mRNA expression by 6-formylindolo [3,2-*b*]carbazole (FICZ), a tryptophan photoproduct (Additional file 11: Figure S9), indicating that each siRNA efficiently inhibited the functional properties of the AHR complex, further suggesting that rVpr-induced L1-RTP depends on AhR, but not ARNT1.

To determine the importance of the LxxLL motif of Vpr for the induction of L1-RTP, we investigated the activity of a Vpr mutant containing AQQAA instead of LQQLL (LA mutant, "LAM" in Figure 5). First, studies of forced expression of wild-type Vpr (WT Vpr) and the LA mutant revealed that the mutant was not active for induction of L1-RTP (Figure 5E, left panel), although comparable levels of each protein were detected (Figure 5E, right panel). Additionally, IP-WB

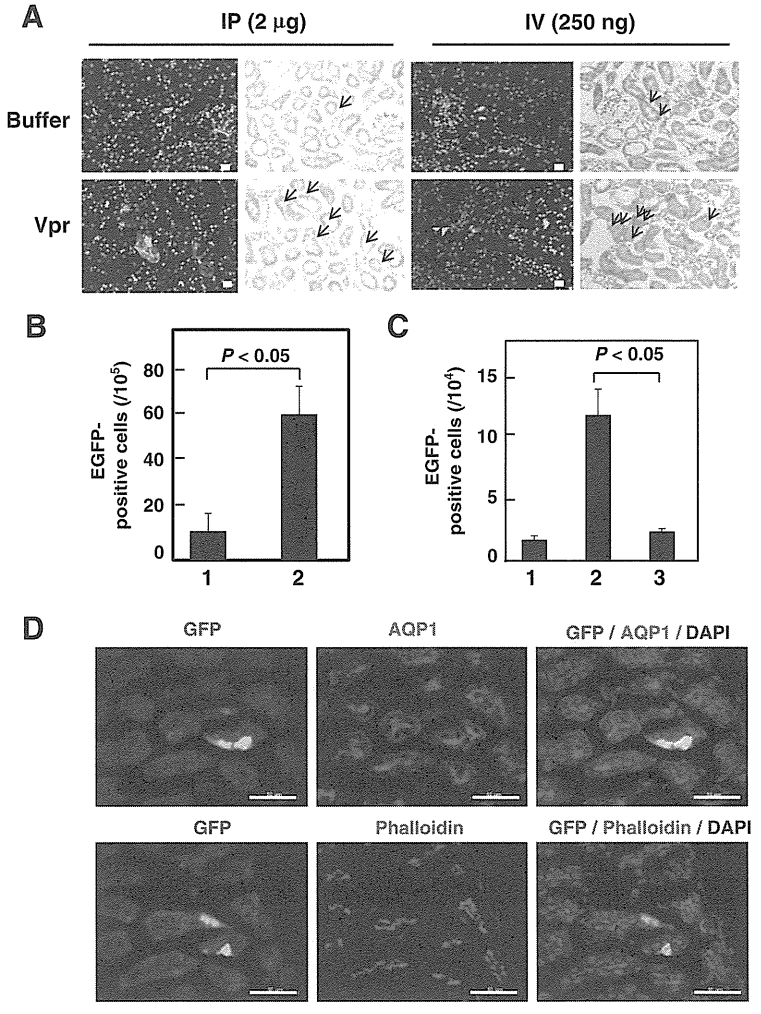

Figure 4 rVpr induces L1-RTP in proximal RTECs. A. Detection of rVpr-induced L1-RTP in kidneys. Immunohistochemical analysis using α-GFP was performed. hL1-Tg mice were administered once with 2 μg rVpr intraperitoneally (left four panels) or 250 ng rVpr intravenously (right panels). Upper panels, buffer control; lower panels, rVpr. Green, EGFP-positive cells; blue, Hoechst 33258 staining. Histology after H/E staining was also depicted. Bar, 20 μm (×200). Arrow, EGFP-positive cells. **B.** Induction of L1-RTP in kidney. Results after six times intravenous injections of 10 ng rVpr were shown. Column 1, buffer control; column 2, rVpr. For each sample, three different slices were prepared and the immunohistochemical analysis was done. Obtained numbers of EGFP-positive cells were then subjected to statistical analysis. $P < 0.05$. **C**. rVpr induced L1-RTP was blocked by 4′-Ed4T. Effects of 4′-Ed4T on the induction of L1-RTP by rVpr were examined using #4 hL1-Tg mice. Mice were intravenously injected with 250 ng rVpr six times. To examine the effects of 4′-Ed4T, the compound of 50 μmoles was intraperitoneally injected 2 h prior to injection of rVpr. The inhibitory effects of 4′-Ed4T were statistically significant ($P < 0.05$). Column 1, buffer; column 2, 250 ng rVpr; column 3, 250 ng rVpr + 4′-Ed4T. **D**. rVpr induced L1-RTP in proximal RTECs. Double staining with α-AQP1 or α-phalloidin was performed. Bar, 50 μm (×400). hL1-Tg mice were intravenously injected with 10 ng rVpr six times. In this experiment, no EGFP-positive cells were detected in the control kidney of mouse that was injected with buffer.

analysis detected an association between WT-Vpr and AhR (Figure 5F, lane 5), but less interaction of the LA mutant with AhR (Figure 5F, lane 6). These data suggest that Vpr-induced L1-RTP is dependent on a molecular interaction with AhR via the LxxLL motif of Vpr.

To identify additional cellular factors involved in rVpr-induced L1-RTP, we investigated the involvement of MAPK, because our previous work revealed that Vpr induced IL-6 production via activation of p38 [7]. First, qPCR analysis revealed that the MAPK inhibitors attenuated rVpr-induced L1-RTP to the basal level observed after treatment with control buffer (Figure 6A, see also Additional file 12: Figure S10 for representative qPCR data). Data indicate that the tested compounds inhibited the up-regulation of L1-RTP by rVpr.

In a previous study, we showed that p38 and C/EBP-β are important for understanding the cellular response to exogenously applied rVpr [7], implying that these molecules are also involved in the induction of L1-RTP by

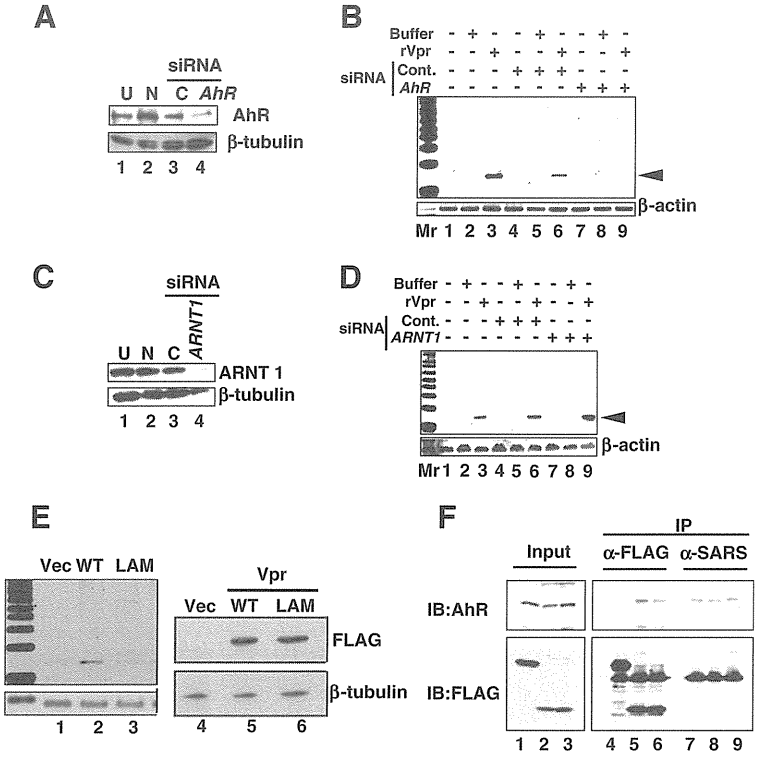

Figure 5 AhR is required for rVpr-induced L1-RTP. A. *AhR* siRNA down-regulated expression of endogenous protein. Lane 1, untreated (U); lane 2, mock transfection without siRNA (N); lane 3, control siRNA (C); lane 4, *AhR* siRNA. **B**. *AhR* siRNA attenuated rVpr-induced L1-RTP. **C**. *ARNT1* siRNA down-regulated expression of endogenous ARNT1 protein. Lane 1, untreated (U); lane 2, mock transfection without siRNA (N); lane 3, control siRNA (C); lane 4, *ARNT1* siRNA. **D**. ARNT1 is dispensable for L1-RTP induction by rVpr. **E**. No induction of L1-RTP by the LA mutant. Left panel. Result of L1-RTP after transfection of plasmid DNA encoding wild-type Vpr (WT) or the LA mutant. Lanes 1 and 4, vector control (Vec); lanes 2 and 5, WT Vpr; lanes 3 and 6, LA mutant (LAM). Right panel. Expression levels of WT Vpr and the LA mutant were comparable. **F**. Association with AhR was impaired in the LA mutant. HEK293T cells were transfected with constructs expressing FLAG-EGFP, FLAG-Vpr-Wt or FLAG-Vpr-LAM. Cell extracts were subjected to IP with α-FLAG followed by WB using α-AhR (upper panel) or α-FLAG (lower panel). Lanes 1, 4 and 7, vector control (FLAG-EGFP); lanes 2, 5 and 8, FLAG-Vpr-Wt; lanes 3, 6 and 9, FLAG-Vpr-LAM. α-SARS mAb was used for control-IP.

rVpr. To confirm this, we focused on the effect of *C/EBP-β* siRNA on rVpr activity. As shown in Figure 6B, transfection of the *C/EBP-β* siRNA down-regulated the endogenous protein level and attenuated rVpr-induced L1-RTP (Figure 6C, lane 9; see also Additional file 10: Figure S8E for data obtained using another siRNA targeting *C/EBP-β* mRNA, which was used in the experiment shown in Figure 6D). In contrast, siRNAs against *CREB* and *c-Jun* did not attenuate rVpr-induced L1-RTP (Figure 6D), although each siRNA efficiently down-regulated endogenous protein expression (Additional file 10: Figure S8F and G). One possible reason is that MAPK inhibitors are not specific for target molecules [37].

Chromatin recruitment of ORF1 induced by rVpr is dependent on AhR

L1 encodes two proteins, open reading frame-1 (ORF1) and ORF2, which are ~40 and ~150 kDa, respectively, and are present in cytoplasmic ribonucleoprotein complexes and cytoplasmic stress granules [50,51]. Moreover, L1-RTP is initiated by target-primed reverse transcription within the genome [9], and ORF1 functions as a nucleic acid chaperone during L1-RTP [52]. These observations suggest that ORF1 is recruited to the chromatin fraction in response to rVpr treatment. To demonstrate chromatin recruitment of ORF1, we transfected a plasmid DNA that encodes ORF1 into HuH-7 cells, and then carried out WB analysis of the chromatin fraction of the transfected cells after treatment of rVpr. The rVpr-induced chromatin recruitment of ORF1 was blocked by MAPK inhibitors examined (Figure 7A, lanes 4 and 6) and the *AhR* siRNA (Figure 7B, lane 4; see also Additional file 13: Figure S11 for results from an independent experiment performed using a different *AhR* siRNA). To further show that ORF1 and AhR form a complex, we transfected a plasmid DNA encoding a chimeric protein of ORF1 and EGFP (pORF1-EGFP) into HuH-7 cells, and then performed IP-WB analysis. IP using α-AhR followed by WB analysis

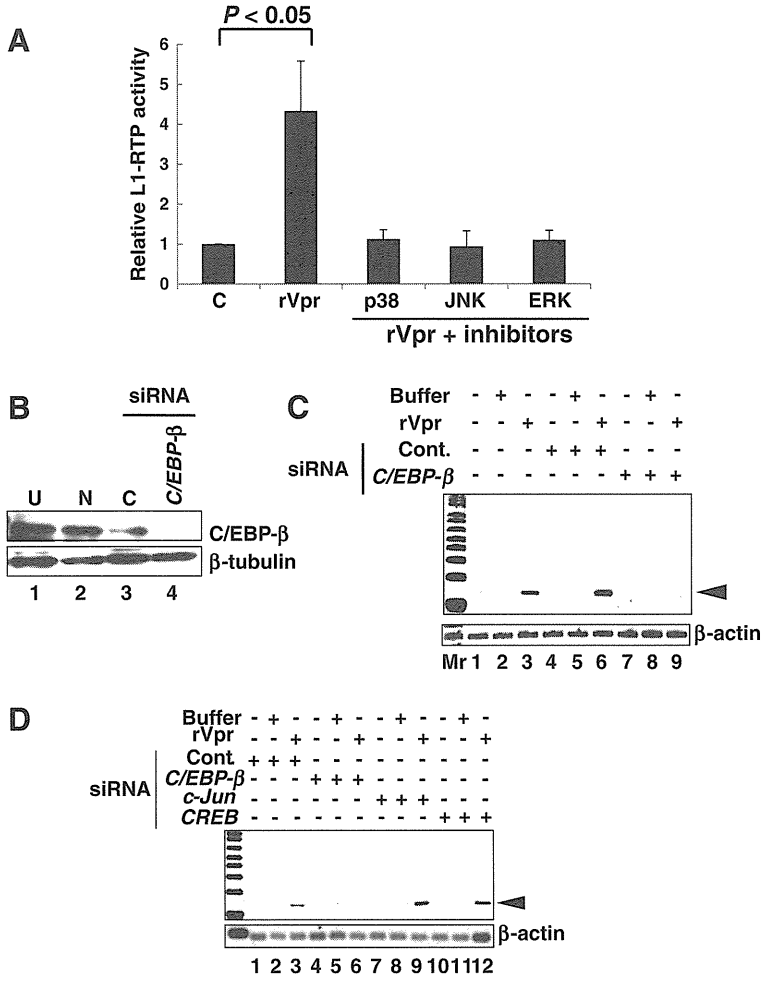

Figure 6 Involvement of MAPK in rVpr-induced L1-RTP. A. Inhibition of rVpr-induced L1-RTP by MAPK inhibitors. Before addition of rVpr, SB202190, SP600125 and PD98059, which were inhibitors of p38, JNK and ERK, respectively, were added. Results of the qPCR assay was shown. **B**. Expression of endogenous C/EBP-β is reduced by siRNA application. See also Additional file 10: Figure S8E showing results obtained by different siRNA. Lane 1, untreated (U); lane 2, mock transfectant (N); lane 3, control siRNA (C); lane 4, *C/EBP-β* siRNA. **C**. Inhibition of rVpr-induced L1-RTP by *C/EBP-β* siRNA. Mr, molecular weight marker. **D**. c-Jun and CREB were dispensable for rVpr induced L1-RTP. rVpr induced L1-RTP was investigated after the introduction of siRNAs targeting c-Jun and CREB. C/EBP-β siRNA was included as positive control. This experiment was done using *C/EBP-β* siRNA different from that used in Figures 6B and C. Effects of each siRNA on the expression of endogenous proteins were depicted in Additional file 10: Figures S8F and S8G.

using α-EGFP revealed that ORF1 and AhR were associated (Figure 7C, lane 2). The reverse experiment, in which IP using α-EGFP was followed by WB using α-AhR, confirmed formation of this complex (Figure 7C, lane 5). The interaction between ORF1 and AhR was also detected in cells in which both ORF1 and ORF2 proteins were expressed exogenously (Additional file 14: Figure S12).

Previously, we reported that FICZ is a potent activator of L1-RTP, and that its activity was dependent on ARNT1, but not on AhR [37]. To determine the functional link between ORF1 and ARNT1, we performed IP-WB analysis after transfecting pORF1-EGFP into HuH-7 cells. ORF1 was detected in an extract of cells treated with FICZ and was recovered using α-ARNT1 (Figure 7D, upper panel, lane 10). By contrast, it was not recovered from extracts of cells treated with rVpr using α-ARNT1 (Figure 7D, upper panel, lane 12). Consistent results were obtained in a reverse experiment, in which WB using α-ARNT1 was performed on a sample recovered by IP using α-EGFP (Figure 7D, lower panel). In this case, the cell extract obtained after FICZ treatment yielded a positive signal (Figure 7D, lower panel, lane 10). These data suggest that the association between ORF1 and ARNT1 is induced by exogenous FICZ but not rVpr.

Discussion

rVpr-induced L1-RTP depends on an AhR-p38-C/EBP-β cellular cascade

Here we found that Vpr is a viral protein active for the induction of L1-RTP. Experiments using MNF, siRNAs

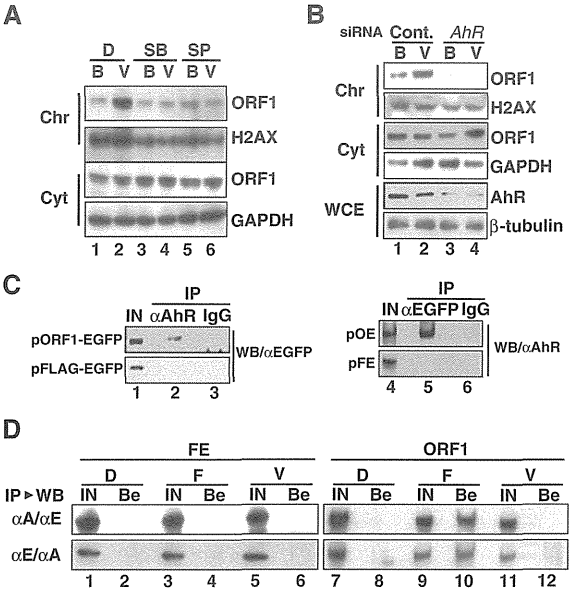

Figure 7 rVpr-induced chromatin recruitment of ORF1. A. Chromatin recruitment of ORF1 is dependent on MAPK. HuH-7 cells were transfected with pORF1-TAP, and then WB was performed using a peroxidase-conjugated human IgG, α-H2AX and α-GAPDH. Cellular fractions of chromatin (Chr) and the cytoplasm (Cyt) were analyzed. D, DMSO; SB, SB202190; SP, SP600125; B, buffer; V, rVpr (5 ng/mL). **B.** *AhR* siRNA blocked rVpr-induced ORF1 chromatin recruitment. After transfection of *AhR* siRNA, similar experiments to those shown in Figure 7A were conducted. Chr, chromatin fraction; Cyt, cytoplasmic fraction; WCE, whole-cell extracts; B, buffer; V, rVpr. See also Additional file 13: Figure S11 showing results of independent experiments done using a different *AhR* siRNA. **C.** Association of AhR and ORF1. HuH-7 cells were transfected with constructs expressing a chimeric protein of ORF1 and EGFP (pORF1-EGFP) or a FLAG-tagged EGFP (pFLAG-EGFP). IP-WB was then performed using α-AhR followed by WB using α-EGFP (lane 2). As a reverse experiment, IP using α-EGFP was performed followed by WB using α-AhR (lane 5). **D.** rVpr induced no association of ORF1 and ARNT1. HuH-7 cells were transfected with pFLAG-EGFP (FE) (lanes 1–6) or pORF1-EGFP (ORF1) (lanes 7–12). After treatment of cells with rVpr (lanes 5, 6, 11, and 12) or FICZ (lanes 3, 4, 9 and 10), IP followed by WB were performed using α-ARNT1 and α-EGFP, respectively (upper panels). As a reverse experiment, IP using α-EGFP followed by WB using α-ARNT1 were performed (lower panels). D, DMSO; F, FICZ (10 nM); V, rVpr (5 ng/mL); IN, input; Be, fraction recovered using protein-G beads.

targeting *AhR* and *C/EBP-β* mRNAs, and MAPK inhibitors revealed that rVpr-induced L1-RTP depends on an AhR-p38-C/EBP-β cellular cascade (Figures 5 and 6). We confirmed by *in vitro* experiments that rVpr did not increase expression of *L1* mRNA or the splicing efficiency of an immature *EGFP* transcript derived from the reporter L1 construct (Additional file 15: Figure S13). Moreover, no apparent changes in the CpG methylation status were observed in the 5′UTR of the exogenous hL1 gene in the kidneys of hL1-Tg mice that had been treated with rVpr (Additional file 8: Figure S6). Our data suggest that rVpr-induced L1-RTP is controlled at the post-transcriptional level, although it has been proposed that L1-RTP is influenced at the transcriptional level by the methylation status of the L1-5′UTR [53,54].

In addition to the LA mutant, we investigated the activity of a Vpr mutant lacking the C-terminal 12 amino acids (ΔC12). A PCR-based assay revealed that the ΔC12 mutant was not active for the induction of L1-RTP (Additional file 16: Figure S14). It has been shown that Vpr has an affinity for nucleic acids, which is attributable to the basic moiety in the C-terminal region of Vpr [55]. To exclude the possibility that the induction of AhR-dependent L1-RTP by Vpr depends on binding to nucleic acids, we investigated the interaction between Vpr and AhR after nuclease treatment. IP-WB analysis combined with treatment with benzonase, a nuclease that degrades both DNA and RNA, revealed that their interaction was not reduced (Additional file 17: Figure S15A). Additionally, ORF1 and AhR constitutively formed a complex, and their interaction was also resistant to nuclease treatment (Additional file 17: Figure S15B). Moreover, rVpr triggered chromatin recruitment of ORF1 in an AhR-dependent manner (Figure 7B). Taken together, these data suggest that Vpr functions as an AhR ligand, and activates a cellular cascade for the induction of L1-RTP.

Biologically active Vpr is present in the blood of HIV-1-positive patients

We detected L1-RTP-inducing activity in the blood of HIV-1 patients: 6 of 15 patients were positive for the induction of L1-RTP (Figure 2A). The L1-RTP activity in those six patients was selectively blocked by 8D1, a mAb against Vpr (Figure 2B). Interestingly, we previously examined blood Vpr by IP-WB analysis, and detected Vpr in 20 of 52 blood samples from HIV-1 patients [4]. Interestingly, the positive frequencies observed in these two sets of experiments are comparable, but greater numbers of samples are needed to conclude that blood Vpr is exclusively biologically active. Although it was reported that an antibody against Vpr is present in patients' blood [56], and implied that Vpr activity would be blocked by such autoantibodies, our current experiments proved that blood Vpr is active for the induction of L1-RTP. Because L1-RTP can alter cellular properties by inducing DNA damage and apoptosis [9], it is tempting to speculate that blood Vpr can modify clinical outcomes of AIDS patients.

Consistent with our previous observation that Vpr protein was detectable in blood samples from HIV-1-positive patients with low viral titres [4], we here detected Vpr-induced L1-RTP in samples from patients with low viral titres. As shown in Figure 2, L1-RTP-inducing activity was detected in some blood samples, and IP-WB

analysis successfully detected a Vpr signal (no. 15) (Additional file 4: Table S1 and Additional file 5: Figure S4). Intriguingly, however, the viral titre of patient 15 was 140 copies/mL (Figure 2D, closed diamond and Additional file 4: Table S1). By striking contrast, the viral titres of the blood samples from patients 3, 8 and 4 were $>10^4$ copies/mL, but no apparent L1-RTP-inducing activity was detected. Although it remains completely unknown why Vpr was present in patients with low viral titres, one possible explanation would be that Vpr is secreted into the blood from latent foci in patients. *In vitro* experiments support the notion that Vpr is excreted by infected cells and functions as a soluble protein with bystander effects [57].

rVpr is active for the induction for L1-RTP *in vivo*

Repeated intravenous administration of 10 ng of rVpr, a dose comparable to patients' blood levels [7], induced L1-RTP *in vivo* (Figure 4B). We observed that administration of rVpr induced L1-RTP in various organs, such as the lymph nodes and spleen. Additionally, we found that Vpr also induced L1-RTP in the kidney (Figure 4A and Additional file 6: Table S2). Notably, even a single injection of 250 ng of rVpr into the tail vein induced L1-RTP in the kidneys (Figure 4A, right panels), suggesting that the kidney is a target organ of Vpr-induced L1-RTP. Immunohistochemical analysis showed that Vpr induced L1-RTP in RTECs, especially in proximal RTECs (Figure 4D). Previously, it was reported that Vpr and Nef are candidate mediators of HIVAN: forced expression of these viral genes in mouse podocytes resulted in proteinuria and glomerular diseases [34]. Although it was proposed that renal dysfunction is a direct effect of primary HIV-1 infection in RTECs [58], it remains to be investigated whether repeated administration of rVpr causes renal insufficiency.

HIVAN develops mostly in people of African descent, and shows the strong influence of genetic traits [59-61]. However, its mechanism remained completely unknown. Importantly, HIVAN has no apparent correlation to viral load [31], and, intriguingly, it has been proposed that the kidneys are a latent reservoir of HIV-1 [62,63]. Based on these observations, it is plausible that both blood-circulating Vpr and Vpr secreted locally from a latent reservoir (the kidney, for example) attack RTECs. To prove this, further studies are required to determine whether the kidney is an organ from which Vpr is constitutively secreted.

In addition to their clinical relevance for HIV-1 pathogenesis, our findings should have a general impact on the involvement of L1-RTP in human diseases. By analysis of tumors using second-generation sequencing technology, *de novo* L1 insertions were detected in the vicinity of tumor suppressor genes [21,22], suggesting that L1 insertion was actively involved in carcinogenesis. Additionally, it was shown that de-regulation of L1-RTP is positively linked to the development of autoimmune diseases [27]. Although these lines of evidence revealed that L1-RTP is induced in somatic cells and is involved in the development of human diseases, it remained unclear how L1-RTP is induced in somatic cells. It was previously reported that 2-amino-1-methyl-6-phenylimidazo[4,5-*b*] pyridine (PhIP), a food-borne carcinogen, induced L1-RTP in the mouse mammary gland, a target organ of carcinogenesis, when it was administered orally to hL1-Tg mice [29]. Given that PhIP is present in broiled meat [64] and has been detected in human breast milk [65], it is plausible that humans are susceptible to the induction of L1-RTP by environmental factors. Further study is required to demonstrate the activity of L1-RTP under pathological conditions, enabling the roles of L1-RTP in disease development to be specified.

Conclusions

Six of the 15 blood samples from HIV-1-positive patients examined were positive for Vpr-induced L1-RTP. L1-RTP-inducing activity was detected in blood samples with low viral titres. Monitoring circulating Vpr in relation to clinical outcomes is important to clarify the roles of Vpr in AIDS symptoms. The present study is the first to show that L1-RTP-inducing activity is present *in vivo*, shedding light on the possible involvement of L1-RTP in human diseases. In further research, it will be important to detect L1-RTP-inducing activity under pathological conditions.

Methods

Chemicals and cells

HuH-7 cells (RCB1366) and HEK293T cells (RCB2202) were obtained from the Riken BioResource Centre Cell Bank. They were cultured in Dulbecco's modified Eagle's medium supplemented with 10% fetal calf serum (Sigma-Aldrich, St. Louis, MI, USA). The transfection efficiencies were ~70 and ~30%, respectively, as determined by fluorescence-activated cell sorting (FACS) on day 2 after transfection of plasmid DNA encoding enhanced green fluorescent protein (EGFP) (data not shown). MNF was kindly provided by Dr. Gabriele Vielhaber (Symrise, Holzminden, Germany). SB20358, SP60012, PD98059 and lipopolysaccharide (L8274) were from Sigma-Aldrich. FICZ was obtained from Enzo Life Sciences (Plymouth Meeting, PA, USA). Protease inhibitors (Roche Diagnostics, Tokyo, Japan) were also purchased.

Antibodies against AhR, (Santa Cruz Biotechnology, Santa Cruz, CA, USA), ARNT1 (Santa Cruz Biotechnology), β-tubulin (Thermo Fisher Scientific, Waltham, MA, USA), H2AX (Millipore, Billerica, MA, USA), C/EBP-β (Cell Signaling Technology Inc., Danvers, MA, USA),

FLAG (Sigma-Aldrich), EGFP (rabbit antibody: Medical & Biological Laboratories, Co., Ltd., Nagoya, Japan; mouse monoclonal antibody: Abcam, Cambridge, United Kingdom), aquaporin 1 (AQP1; Abcam) and glyceraldehyde 3-phosphate dehydrogenase (GAPDH; Trevigen, Gaithersburg, MD, USA) were used as the primary antibodies. A rabbit polyclonal antibody against human ORF1 was generated using the peptide MGKKQNRKTGNSK TQSAC (amino acids denoted by single letters) as an immunogen (Medical & Biological Laboratories). An Alexa Fluor 546-conjugated antibody to phalloidin (Invitrogen, Carlsbad, CA, USA) was purchased. As secondary antibodies, α-mouse IgG (GE Healthcare Bio-Sciences Corp., Piscataway, NJ, USA), α-rabbit IgG (GE Healthcare), and α-goat IgG (Santa Cruz Biotechnology), all of which were conjugated with horseradish peroxidase, were used. For immunohistochemical analysis, Alexa Fluor 555-conjugated goat α-rabbit IgG (Invitrogen) and Alexa Fluor 488 goat α-mouse IgG (Invitrogen) were used as the secondary antibodies. Hoechst 33258 was purchased from Invitrogen.

Based on recent reports that RTIs efficiently blocked L1-RTP [39,40], we used 4′-Ed4T, which has more potent inhibitory activity than d4T and less effect on DNA polymerases, and which is currently undergoing phase IIb clinical trials in HIV-1-infected patients [41]. Two hours before injection of rVpr, 50 μmoles of 4′-Ed4T was injected intraperitoneally to give a final concentration of approximately 25 μM when most of the compound is transferred to the blood, the estimated volume of which is ~2 mL.

Purification of rVpr and assays of L1-RTP

rVpr was expressed using pGEX-6P-1 in *Escherichia coli* BL21 and purified as described previously (Figure 1A) [4]. Purified rVpr was tested for endotoxin using a highly sensitive lipopolysaccharide (LPS) assay with Limulus amebocyte lysate, the detection limit of which was 0.25 EU/mL (Wako Pure Chemical Ind., Ltd., Osaka, Japan). For L1-RTP assays, we used two reporter constructs, pEF06R [38] and pCEP4/L1mneoI/ColE1 (pL1-Neo^R) [28,35-37], for semi-quantitative and quantitative PCR, and colony formation assays, respectively. Each construct contained all components of human L1 with single transcriptional units with EGFP or Neo^R, which were inserted in reverse orientation. When L1-RTP occurs, the intron within each reporter gene is spliced out, and then pEF06R expresses functional EGFP, whereas pL1-Neo^R expresses a functional neomycin-resistance gene (Neo^R). Cells were transfected with pEF06R or pL1-Neo^R using Lipofectamine 2000 (Invitrogen) or Xfect (Takara Bio Inc., Shiga, Japan). Cells were selected for 2 days with puromycin (Puro, 0.5 μg/mL) for pEF06R, or with hygromycin (Hygro, 25 μg/mL) for pL1-Neo^R. Next, cells were treated for additional 2 or 3 days with the indicated amounts of rVpr.

For the PCR assay, genomic DNA was prepared from harvested cells using a DNA extraction system (QuickGene; Fujifilm, Tokyo, Japan). For semi-quantitative PCR, primers that were designed for each exon would amplify a product of ~1040 bp, whereas they would generate a product of ~140 bp upon L1-RTP. Thus, occurrence of L1-RTP was determined by evaluating the size of the amplified product [28,29,37]. After staining of amplified DNA with SYBR Green I (LONZA, Basel, Switzerland), signal intensities of the 140 bp bands were measured using a molecular imager (FX-PRO; Bio-Rad, Hercules, CA, USA) and normalized by the signal intensity of the β-actin band, used as the internal control. Relative intensities (RIs) of each 140 bp band were calculated by standardizing the signal of the buffer-treated sample as "1".

For qPCR analysis, 5′-GAA CGG CAT CAA GGT GAA CT-3′ and 5′-GGG GTG TTC TGC TGG TAG TG-3′, which were designed for each exon of the *EGFP* gene, were used as forward and reverse primers, respectively. A TaqMan-probe (5′-FAM- TGC AG * C TGG CCG AC -MGB-3′) (Invitrogen) was used to detect an amplicon of 87 bp in length (* denotes the exon junction). Template DNA was amplified with Eagle Taq Master Mix (Roche Diagnostics) and a CFX Connect Real-Time System (Bio-Rad) using the following amplification conditions: 95°C for 10 min, followed by 45 cycles of 95°C for 15 sec and 64°C for 15 sec. To obtain a standard curve for EGFP-qPCR, *EGFP* DNA generated after the induction of L1-RTP was amplified using the above primers and cloned into the pGEM-T Easy vector (Promega, Madison, USA). After confirmation of the nucleotide sequence, standard samples were prepared by mixing human or mouse genomic DNA with the *EGFP*-containing plasmid to give 1.0, 10^{-1}, 10^{-2}, 10^{-3} and 10^{-4} copies/cell. To normalize the amounts of input DNA, human β-globin or mouse β-actin was quantified by qPCR with SYBR Premix Ex Taq (TaKaRa) and the CFX Connect Real-Time System (Bio-Rad). For human β-globin, the forward primer was 5′-TTG GAC CCA GAG GTT CTT TG-3′ and the reverse primer was 5′-GAG CCA GGC CAT CAC TAA AG-3′; for mouse β-actin, the forward primer was 5′-TGA CGT TGA CAT CCG TAA AGA CC-3′ and the reverse primer was 5′-AAG GGT GTA AAA CGC AGC TCA-3′.

In the colony formation assay, ~2.0×10^6 cells were transfected with pL1-Neo^R and selected with 25 μg/mL Hygro, and 1.0×10^5 cells were re-plated to new plates (Split). Next, cells were treated for 2 days with rVpr and further cultured in the presence of neomycin (800 μg/mL) [35-37]. In the initial experiment, we used 5–10 ng/mL rVpr because the maximum reported plasma Vpr

concentration in HIV-1-positive patients is ~5 ng/mL [4]. To determine Vpr activity for L1-RTP induction, each of the six plates was treated with rVpr or a buffer control for 2 days, and further cultured in the presence of neomycin. After 3–4 weeks, cell aggregates were stained with methylene blue, and colonies were enumerated. To minimize plate-to-plate variation, the colony numbers of the middle four of the six plates were subjected to statistical analysis. At least two independent experiments were performed, representative results of which are shown.

Suppression of rVpr-induced L1-RTP by mAbs against Vpr

The effects of mAbs against Vpr on the induction of L1-RTP were investigated by applying 5 ng of rVpr with 500 ng of 8D1 and C217 [4], giving an approximately 10-fold excess molar amount of rVpr. After 60 min of incubation at room temperature, a 300 μL reaction mixture was filtrated and added to 1.5 mL of culture medium of cells. As a control, a SARS mAb, an irrelevant mAb that recognizes a spike protein of the severe acute respiratory syndrome corona virus (SARS-CoV), was used.

Effect of down-regulation of endogenous proteins on induction of L1-RTP

For each gene, two small interfering RNAs (siRNAs) were prepared (Applied Biosystems, Foster City, CA, USA or Thermo Scientific), and their functions were evaluated by transfection into cells followed by WB analysis. The nucleotide sequences of each siRNA are shown in Additional file 18: Table S3. To evaluate the inhibitory effects of the siRNAs on L1-RTP induction, each siRNA was introduced on day 3 after initial transfection with pL1-Neo^R or pEF06R. Two days later, the cells were re-plated, incubated for 2 days with rVpr, and subjected to analysis. Silencer Negative Control siRNAs (cat. no. AM4613, AM4637 and AM464; Life Technologies Corporation, Carlsbad, CA, USA) were used as controls.

Effects of MAP kinase inhibitors on rVpr-induced L1-RTP

HuH-7 cells were transfected with pEF06R and selected for 2 days with 0.5 μg/mL Puro. On day 3 after transfection, cells were re-plated and subjected to an L1-RTP assay. To examine the effects of MAPK inhibitors, SB202190, SP600125 and PD98059 at concentrations of 1, 100 and 20 μM, respectively, were added 1 h before the addition of rVpr. The cells were exposed to 10 ng/mL rVpr for 3 days and subjected to qPCR analysis. Genomic DNA was isolated using the QuickGene DNA Tissue Kit S and QuickGene-800 (Fujifilm). To selectively detect *EGFP* genes derived from L1-RTP, ~250 ng of DNA were used as the qPCR template. To amplify *β-globin* gene as an internal control, ~50 ng of DNA were used as the qPCR template.

Administration of rVpr to hL1-Tg mice and L1-RTP assessment

For *in vivo* experiments, we used two transgenic mouse lines, #4 and #67, in which the L1-DNA fragment of pEF06R had been introduced as a transgene (hL1-Tg mice; Figure 1A, sidebar) [28,29]. These two lines were selected because they display low background L1-RTP during embryogenesis but respond vigorously to environmental compounds [29]. The CpG island of the 5′ untranslated region of introduced human L1 (L1-5′UTR) was highly methylated in #4 and #67 mice, as assessed by a PCR-based assay using methylation-specific primers [29]. All animal experiments were approved by the Animal Care and Use Committee at the National Center for Global Health and Medicine (NCGM).

Clinical samples

Fifteen blood samples obtained from anti-retroviral therapy-naïve male patients who presented to the NCGM hospital between October 1996 and October 2003 were subjected to the PCR-based assay. The patients were 21–44 years of age with viral loads and CD4 counts of 50–230,000 copies/mL and 315–795 cells/mL, respectively. Nine healthy volunteers served as controls. To detect L1-RTP-inducing activity, HEK293T cells were first transfected with pEF06R and selected with 0.5 μg/mL Puro. Then, 150 μL of each heat-inactivated patient serum sample was added to 1.35 mL of culture medium of HEK293T cells. To show that L1-RTP activity in patients' blood was attributable to Vpr, 100 μL of serum was reacted for 60 min with 500 ng of 8D1 or SARS-S mAb at room temperature in a 300 μL reaction volume. The experimental protocol was approved by the institutional review board of NCGM.

L1-RTP activity of the Vpr mutant

The LA mutant, which contains AQQAA at codons 64–68, and wild-type (WT) Vpr were expressed as FLAG-tagged proteins using the pFLAG-CMV2 expression vector (Sigma-Aldrich). To obtain comparable levels of expression of each protein, the molar ratio of 1:4 of plasmid DNA for the wild-type Vpr and the LA mutant were transfected respectively. On the next day of transfection, cells were subjected to the PCR-based assay.

Chromatin recruitment of ORF1 induced by rVpr

We used the pORF1-TAP (tandem affinity purification) construct [66], which encodes a chimeric protein of ORF1, protein A and calmodulin-binding protein. On day 2 after transfection of pORF1-TAP into HuH-7 cells, 5 ng/mL rVpr was added to the culture medium, and cell extracts were prepared on the following day. The chromatin-enriched fraction (chromatin fraction) was

isolated using a Subcellular Protein Fractionation Kit (Thermo Fisher Scientific) with micrococcal nuclease, as described previously [29]. Detection of ORF1-TAP was performed by probing with a horseradish peroxidase-conjugated human IgG (Jackson ImmunoResearch West Grove, PA, USA). H2AX was used as an internal control for the chromatin fraction.

ORF1, AhR, and Vpr complex formation

HuH-7 or HEK293T cells were transfected with the plasmid constructs pFLAG-Vpr-Wt or pFLAG-Vpr-LA mutant, pORF1-EGFP and pFLAG-EGFP, which encode FLAG-tagged Vpr, a chimeric protein of ORF1 and EGFP, and FLAG-tagged EGFP, respectively. On day 2 after transfection, cells were treated with 10 ng/mL rVpr for 1 day to evaluate the dependence of the protein-protein interaction on Vpr. Then, cells were subjected to IP-WB analysis. To analyze the ORF1-AhR association, cells were suspended in a buffer containing 50 mM Tris (pH 7.5), 150 mM NaCl, 1% NP40, 1 mM EDTA and a protease inhibitor cocktail and subjected to brief sonication. For analysis of the Vpr-AhR association, cells were suspended in a buffer containing 25 mM HEPES (pH 7.5), 200 mM NaCl, 0.1% NP40, 10% glycerol and a protease inhibitor cocktail, and were completely lysed by passage through 22 G and 27 G needles (in that order) ten times. Cell extracts (500 to 2000 μg) were pre-cleared with protein G Sepharose beads (GE Healthcare), reacted with 4 μg of α-AhR, α-EGFP, α-FLAG or α-SARS, and then recovered with protein G beads. As an "input" sample, about 5 or 10% of each extract subjected to immunoprecipitation, was assessed simultaneously.

Immunohistochemical analysis of EGFP-positive cells

After perfusion fixation, organs were immersed in 0.1 M phosphate buffer (PB) (pH 7.4) supplemented with 4% paraformaldehyde at 4°C. On the following day, samples were serially immersed at 4°C in PB supplemented with 10% saccharose for 1 h, 20% saccharose until immersed completely, and then 30% saccharose overnight. Next, samples were embedded in Optimal Cutting Temperature compound (Sakura Finetek, Torrance, CA, USA) for cryosectioning. Using a cryostat (Leica Biosystems, Wetzlar, Germany), three slices (5 μm thick) were prepared from different sections of the fixed kidney: a first slice from the middle part of the kidney, a second section is from the part that contained mainly cortex with little amount of medulla, and the third section that is composed mainly of cortex. Samples were washed three times with 0.1 M phosphate-buffered saline (PBS) (10 min per wash), and incubated for 30 min at room temperature in Image-iT Fx signal enhancer (Invitrogen). After rinsing three times with 25 mM Tris-HCl (pH 7.5), 150 mM NaCl, and 0.05% Tween 20 (TBST) (10 min each), sections were then reacted with rabbit α-EGFP antibody (1:2000; Medical & Biological Laboratories) in TBST supplemented with 1% bovine serum albumin (BSA) at 4°C. On the following day, specimens were rinsed three times with TBST, and then incubated with Alexa Fluor 555-conjugated goat α-rabbit IgG antibody (1:5000; Invitrogen) for 2 h at room temperature. Nuclear DNA was stained with Hoechst 33258 at a final concentration of 0.36 μM. Fluorolabeled sections were examined under a fluorescence microscope (Olympus BX51; Olympus, Tokyo, Japan). Using the cellSens system (Olympus), total cell numbers in each section were first counted automatically. Next, numbers of EGFP-positive cells were counted manually. The frequency of EGFP-positive cells was calculated using the numbers of total and EGFP-positive cells. Three independent sections were prepared from a single specimen and subjected to analysis. The significance of the frequency of EGFP-positive cells was then evaluated statistically.

To identify RTECs positive for L1-RTP, immunohistochemistry was performed as described previously [42] using the following primary antibodies; α-GFP antibody (1:200 dilution) (Abcam, UK), α-AQP1 antibody (1:200 dilution) [43], and Alexa Fluor 546-phalloidin (1:400 dilution) (Invitrogen) [44].

L1-5'UTR methylation status

We performed sodium bisulfite treatment of genomic DNA using the EZ DNA Methylation Kit (Zymo Research, Irvine, CA, USA), according to the manufacturer's instructions. One microlitre of the aliquot was used as the template for combined bisulfite restriction analysis (COBRA) [45]. Primers used for amplification of the L1 transgene promoter region were as follows: forward 5′-GTAAGGGGTTAGGGAGTTTTT-3′ and reverse 5′-CCTTACAATTTAATCTCAAACTA-3′. The PCR reactions were performed in a volume of 20 μL containing 1 μL of bisulfite-treated genomic DNA, primers (0.3 μM each), and a 10 μL EpiTect MSP Kit (Qiagen, Hilden, Germany). The amplification conditions consisted of 40 cycles of 94°C for 15 sec, 50°C for 30 sec and 72°C for 30 sec. PCR products were digested using the restriction enzyme *Taq* I (New England Biolabs, Ipswich, MA, USA), which is specific for the methylated sequence, after sodium bisulfite treatment. Digested products were resolved by 3% agarose gel electrophoresis and stained with ethidium bromide.

Statistical analysis

Statistical significance was evaluated using the Mann-Whitney U-test. A P value < 0.05 was deemed to indicate statistical significance.

Additional file

Additional file 1: Figure S1. No cytotoxicity of rVpr.

Additional file 2: Figure S2. Standard curve of qPCR assay with a TaqMan probe.

Additional file 3: Figure S3. L1-RTP induced by low dose of rVpr.

Additional file 4: Table S1. Summary viral titres and L1-RTP activity.

Additional file 5: Figure S4. Detection of Vpr in blood samples of HIV-1 positive patients.

Additional file 6: Table S2. Summary of the PCR-based assay *in vivo*.

Additional file 7: Figure S5. Effects of d4T on rVpr-induced L1-RTP.

Additional file 8: Figure S6. No changes of methylation status of CpG in the L1-5′UTR.

Additional file 9: Figure S7. Inhibitory effects of MNF on rVpr-induced L1-RTP.

Additional file 10: Figure S8. Effects of siRNAs of *AhR, ARNT1*, *CREB* and *c-Jun* on expression of endogenous proteins.

Additional file 11: Figure S9. *CYP1A1* expression under down-regulation of AhR or ARNT1.

Additional file 12: Figure S10. Effects of MAPK inhibitors on rVpr-induced L1-RTP.

Additional file 13: Figure S11. Effects of AhR siRNA on chromatin recruitment of ORF1.

Additional file 14: Figure S12. Constitutive association of ORF1 and AhR under the conditions competent for the induction of L1-RTP.

Additional file 15: Figure S13. No apparent changes of expression of L1 mRNA after the addition of rVpr.

Additional file 16: Figure S14. L1-RTP by Vpr required a carboxy-terminal region.

Additional file 17: Figure S15. Effects of benzonase on the interaction of AhR and ORF1 or Vpr.

Additional file 18: Table S3. Nucleotide sequence of siRNA used in the current study.

Competing interest

All authors declare that they have no competing interest for the current work.

Authors' contributions

NO, MT, YS, KI, MS, AD and SH carried out biochemical analyzes using cell lines. KY, TO and TD NO, MT, YS, MG, AD and TO performed experiments using hL1-Tg mice. YK, TO, KI and YS established qPCR of L1-RTP. AM and NO analyzed methylation status of CpG in the L1-5′UTR. YS, NO, MT, TI and MY carried out immunohistochemistry of cells positive for rVpr-induced L1-RTP. NO, SH, JT, HG and SO analyzed correlation of the activity of Vpr-induced L1-RTP in blood of HIV-positive patients and clinical manifestations. NO, MB and MT examined the effects of RTIs on rVpr-induced L1-RTP. SK and YI designed experiments. NO, KI, MT, AD, YS and YI were involved in preparation of the manuscript. All authors read and approved the final manuscript.

Acknowledgements

We are grateful to Drs. Elena T. Luning Prak (University of Pennsylvania Medical Center), Gilbert Nicolas (University of Michigan Medical School), and Gabriele Vielhaber (Symrise, Germany) for providing us with pEF06R, pCEP4/L1*mneo*I/ColE1, and MNF, respectively. We thank Ms. Rieko Yanobu-Takanashi for qPCR of the L1 transgenes in the L1-transgenic mice. Mr. Noriyuki Okudaira was an applicant supported by a Grant-in-Aid from the Tokyo Biochemical Research Foundation. This work was supported in part by Grants-in-Aid for Research from the National Center for Global Health and Medicine (22A-113), the Tokyo Biochemical Research Foundation and the Ministry of Health, Labor and Welfare of Japan (09156296).

Author details

[1]Department of Intractable Diseases, Research Institute, National Center for Global Health and Medicine, 1-21-1 Toyama, Shinjuku-ku, Tokyo 162-8655, Japan. [2]Graduate School of Comprehensive Human Sciences, University of Tsukuba, 1-1-1 Ten-nodai, Tsukuba 305-8577, Japan. [3]Department of Laboratory Animal Medicine, Research Institute, National Center for Global Health and Medicine, 1-21-1 Toyama, Shinjuku-ku, Tokyo 162-8655, Japan. [4]Department of Gastroenterology, Research Center for Hepatitis and Immunology, Research Institute, National Center for Global Health and Medicine, 1-7-1 Kohnodai, Ichikawa, Chiba 272-8516, Japan. [5]Department of Tropical Medicine and Malaria, Research Institute, National Center for Global Health and Medicine, 1-21-1 Toyama, Shinjuku-ku, Tokyo 162-8655, Japan. [6]Division of Hematology, Department of Internal Medicine, National Center for Global Health and Medicine, 1-21-1 Toyama, Shinjuku-ku, Tokyo 162-8655, Japan. [7]AIDS Clinical Center, National Center for Global Health and Medicine, 1-21-1 Toyama, Shinjuku-ku, Tokyo 162-8655, Japan. [8]Division of Antiviral Chemotherapy, Center for Chronic Viral Diseases, Graduate School of Medical and Dental Sciences, Kagoshima University, Kagoshima 890-8544, Japan. [9]Department of Nephrology, Graduate School of Medicine, Kyoto University, Shogoin-Kawahara-cho 54, Sakyo-ku, Kyoto 606-8507, Japan. [10]Section of Animal Model, Department of Infectious Diseases, Research Institute, National Center for Global Health and Medicine, 1-21-1 Toyama, Shinjuku-ku, Tokyo 162-8655, Japan. [11]Department of Legal Medicine, Hyogo College of Medicine, 1-1 Mukogawa- cho, Nishinomiya, Hyogo 663-8501, Japan. [12]Kyoto University, Graduate School of Medicine, Medical Innovation Center, Shogoin-Kawahara-cho 53, Sakyo-ku, Kyoto 606-8507, Japan.

Received: 16 November 2012 Accepted: 18 July 2013
Published: 5 August 2013

References

1. Cohen EA, Dehni G, Sodroski JG, Haseltine WA: **Human immunodeficiency virus vpr product is a virion-associated regulatory protein.** *J Virol* 1990, **64**:3097–3099.
2. Kogan M, Rappaport J: **HIV-1 accessory protein Vpr: relevance in the pathogenesis of HIV and potential for therapeutic intervention.** *Retrovirology* 2011, **8**:25.
3. Levy DN, Refaeli Y, MacGregor RR, Weiner DB: **Serum Vpr regulates productive infection and latency of human immunodeficiency virus type 1.** *Proc Natl Acad Sci USA* 1994, **91**:10873–10877.
4. Hoshino S, Sun B, Konishi M, Shimura M, Segawa T, Hagiwara Y, Koyanagi Y, Iwamoto A, Mimaya J, Terunuma H, Kano S, Ishizaka Y: **Vpr in plasma of HIV-1-positive patients is correlated with the HIV-1 RNA titres.** *AIDS Res Hum Retrovir* 2007, **23**:391–397.
5. Patel CA, Mukhtar M, Pomerantz RJ: **Human immunodeficiency virus type 1 Vpr induces apoptosis in human neuronal cells.** *J Virol* 2000, **74**:9717–9726.
6. Muthumani K, Choo AY, Premkumar A, Hwang DS, Thieu KP, Desai BM, Weiner DB: **Human immunodeficiency virus type 1 (HIV-1) Vpr-regulated cell death: insights into mechanism.** *Cell Death Differ* 2005, **12**:962–970.
7. Hoshino S, Konishi M, Mori M, Shimura M, Nishitani C, Kuroki Y, Koyanagi Y, Kano S, Itabe H, Ishizaka Y: **HIV-1 Vpr induces TLR4/MyD88-mediated IL-6 production and reactivates viral production from latency.** *J Leukoc Biol* 2010, **87**:1133–1143.
8. Bannert N, Kurth R: **Retroelements and the human genome: new perspectives on an old relation.** *Proc Natl Acad Sci USA* 2004, **101**:14572–14579.
9. Goodier JL, Kazazian HH Jr: **Retrotransposons revisited: the restraint and rehabilitation of parasites.** *Cell* 2008, **135**:23–35.
10. Brouha B, Schustak J, Badge RM, Lutz-Prigge S, Farley AH, Moran JV, Kazazian HH Jr: **Hot L1s account for the bulk of retrotransposition in the human population.** *Proc Natl Acad Sci USA* 2003, **100**:5280–5285.
11. Kazazian HH Jr, Wong C, Youssoufian H, Scott AF, Phillips DG, Antonarakis SE: **Haemophilia A resulting from de novo insertion of L1 sequences represents a novel mechanism for mutation in man.** *Nature* 1988, **332**:164–166.
12. Hancks DC, Kazazian HH Jr: **Active human retrotransposons: variation and disease.** *Curr Opin Genet Dev* 2012, **22**:1–13.
13. Muotri AR, Chu VT, Marchetto MC, Deng W, Moran JV, Gage FH: **Somatic mosaicism in neuronal precursor cells mediated by L1 retrotransposition.** *Nature* 2005, **435**:903–910.

14. Georgiou I, Noutsopoulos D, Dimitriadou E, Markopoulos G, Apergi A, Lazaros L, Vaxevanoglou T, Pantos K, Syrrou M, Tzavaras T: **Retrotransposon RNA expression and evidence for retrotransposition events in human oocytes.** *Hum Mol Genet* 2009, **18**:1221–1228.
15. Kano H, Godoy I, Courtney C, Vetter MR, Gerton GL, Ostertag EM, Kazazian HH Jr: **L1 retrotransposition occurs mainly in embryogenesis and creates somatic mosaicism.** *Genes Dev* 2009, **23**:1303–1312.
16. Coufal NG, Garcia-Perez JL, Peng GE, Yeo GW, Mu Y, Lovci MT, Morell M, O'Shea KS, Moran JV, Gage FH: **L1 retrotransposition in human neural progenitor cells.** *Nature* 2009, **460**:1127–1131.
17. Baillie JK, Barnett MW, Upton KR, Gerhardt DJ, Richmond TA, De Sapio F, Brennan PM, Rizzu P, Smith S, Fell M, Talbot RT, Gustincich S, Freeman TC, Mattick JS, Hume DA, Heutink P, Carninci P, Jeddeloh JA, Faulkner GJ: **Somatic retrotransposition alters the genetic landscape of the human brain.** *Nature* 2011, **479**:534–537.
18. Iskow RC, McCabe MT, Mills RE, Torene S, Pittard WS, Neuwald AF, Van Meir EG, Vertino PM, Devine SE: **Natural mutagenesis of human genomes by endogenous retrotransposons.** *Cell* 2010, **141**:1253–1261.
19. Ting DT, Lipson D, Paul S, Brannigan BW, Akhavanfard S, Coffman EJ, Contino G, Deshpande V, Iafrate AJ, Letovsky S, Rivera MN, Bardeesy N, Maheswaran S, Haber DA: **Aberrant overexpression of satellite repeats in pancreatic and other epithelial cancers.** *Science* 2011, **331**:593–596.
20. Kazazian HH Jr: **Mobile DNA transposition in somatic cells.** *BMC Biol* 2011, **9**:62.
21. Lee E, Iskow R, Yang L, Gokcumen O, Haseley P, Luquette LJ 3rd, Lohr JG, Harris CC, Ding L, Wilson RK, Wheeler DA, Gibbs RA, Kucherlapati R, Lee C, Kharchenko PV, Park PJ, Cancer Genome Atlas Research Network: **Landscape of somatic retrotransposition in human cancers.** *Science* 2012, **337**:967–971.
22. Shukla R, Upton KR, Muñoz-Lopez M, Gerhardt DJ, Fisher ME, Nguyen T, Brennan PM, Baillie JK, Collino A, Ghisletti S, Sinha S, Iannelli F, Radaelli E, Dos Santos A, Rapoud D, Guettier C, Samuel D, Natoli G, Carninci P, Ciccarelli FD, Garcia-Perez JL, Faivre J, Faulkner GJ: **Endogenous retrotransposition activates oncogenic pathways in hepatocellular carcinoma.** *Cell* 2013, **153**:101–111.
23. Gilbert N, Lutz-Prigge S, Moran JV: **Genomic deletions created upon LINE-1 retrotransposition.** *Cell* 2002, **110**:315–325.
24. Symer DE, Connelly C, Szak ST, Caputo EM, Cost GJ, Parmigiani G, Boeke JD: **Human L1 retrotransposition is associated with genetic instability in vivo.** *Cell* 2002, **110**:327–338.
25. Gasior SL, Wakeman TP, Xu B, Deininger PL: **The human LINE-1 retrotransposon creates DNA double-strand breaks.** *J Mol Biol* 2006, **357**:1383–1393.
26. Haoudi A, Semmes OJ, Mason JM, Cannon RE: **Retrotransposition-competent human LINE-1 induces apoptosis in cancer cells with intact p53.** *J Biomed Biotechnol* 2004, **2004**:185–194.
27. Stetson DB, Ko JS, Heidmann T, Medzhitov R: **Trex1 prevents cell-intrinsic initiation of autoimmunity.** *Cell* 2008, **134**:587–598.
28. Okudaira N, Goto M, Yanobu-Takanashi R, Tamura M, An A, Abe Y, Kano S, Hagiwara S, Ishizaka Y, Okamura T: **Involvement of retrotransposition of long interspersed nucleotide element-1 in skin tumorigenesis induced by 7,12-dimethylbenz[a]anthracene and 12-O-tetradecanoylphorbol-13-acetate.** *Cancer Sci* 2011, **102**:2000–2006.
29. Okudaira N, Okamura T, Tamura M, Iijma K, Goto M, Matsunaga A, Ochiai M, Nakagama H, Kano S, Fujii-Kuriyama Y, Ishizaka Y: **Long interspersed element-1 is differentially regulated by food-borne carcinogens via the aryl hydrocarbon receptor.** *Oncogene* 2012. in press.
30. Rao TK, Filippone EJ, Nicastri AD, Landesman SH, Frank E, Chen CK, Friedman EA: **Associated focal and segmental glomerulosclerosis in the acquired immunodeficiency syndrome.** *N Engl J Med* 1984, **310**:669–673.
31. Izzedine H, Wirden M, Launay-Vacher V: **Viral load and HIV-associated nephropathy.** *N Engl J Med* 2005, **353**:1072–1074.
32. Wyatt CM, Meliambro K, Klotman PE: **Recent progress in HIV-associated nephropathy.** *Annu Rev Med* 2012, **63**:147–159.
33. Dickie P, Roberts A, Uwiera R, Witmer J, Sharma K, Kopp JB: **Focal glomerulosclerosis in proviral and c-fms transgenic mice links Vpr expression to HIV-associated nephropathy.** *Virology* 2004, **322**:69–81.
34. Zhong J, Zuo Y, Ma J, Fogo AB, Jolicoeur P, Ichikawa I, Matsusaka T: **Expression of HIV-1 genes in podocytes alone can lead to the full spectrum of HIV-1-associated nephropathy.** *Kidney Int* 2005, **68**:1048–1060.
35. Gilbert N, Lutz S, Morrish TA, Moran JV: **Multiple fates of L1 retrotransposition intermediates in cultured human cells.** *Mol Cell Biol* 2005, **25**:7780–7795.
36. Wei W, Morrish TA, Alisch RS, Moran JV: **A transient assay reveals that cultured human cells can accommodate multiple LINE-1 retrotransposition events.** *Anal Biochem* 2000, **284**:435–438.
37. Okudaira N, Iijma K, Koyama T, Minemoto Y, Kano S, Mimori A, Ishizaka Y: **Induction of long interspersed nucleotide element by 6-formylindolo [3,2-*b*]carbazole, a tryptophan photoproduct.** *Proc Natl Acad Sci USA* 2010, **107**:18487–18492.
38. Farkash EA, Kao GD, Horman SR, Prak ET: **Gamma radiation increases endonuclease-dependent L1 retrotransposition in a cultured cell assay.** *Nucleic Acids Res* 2006, **34**:1196–1204.
39. Jones RB, Garrison KE, Wong JC, Duan EH, Nixon DF, Ostrowski MA: **Nucleoside analogue reverse transcriptase inhibitors differentially inhibit human LINE-1 retrotransposition.** *PLoS One* 2008, **3**:e1547.
40. Dai L, Huang Q, Boeke JD: **Effect of reverse transcriptase inhibitors on LINE-1 and Ty1 reverse transcriptase activities and on LINE-1 retrotransposition.** *BMC Biochem* 2011, **12**:18.
41. Yang G, Dutschman GE, Wang CJ, Tanaka H, Baba M, Anderson KS, Cheng YC: **Highly selective action of triphosphate metabolite of 4′-ethynyl D4T: a novel anti-HIV compound against HIV-1 RT.** *Antiviral Res* 2007, **73**:185–191.
42. Asada N, Takase M, Nakamura J, Oguchi A, Asada M, Suzuki N, Yamamura K, Nagoshi N, Shibata S, Rao TN, Fehling HJ, Fukatsu A, Minegishi N, Kita T, Kimura T, Okano H, Yamamoto M, Yanagita M: **Dysfunction of fibroblasts of extrarenal origin underlies renal fibrosis and renal anemia in mice.** *J Clin Invest* 2011, **121**:3981–3990.
43. Tanaka M, Endo S, Okuda T, Economides AN, Valenzuela DM, Murphy AJ, Robertson E, Sakurai T, Fukatsu A, Yancopoulos GD, Kita T, Yanagita M: **Expression of BMP-7 and USAG-1 (a BMP antagonist) in kidney development and injury.** *Kidney Int* 2008, **73**:181–191.
44. Nürnberger A, Räbiger M, Mack A, Diaz J, Sokoloff P, Mühlbauer B, Luippold G: **Subapical localization of the dopamine D3 receptor in proximal tubules of the rat kidney.** *J Histochem Cytochem* 2004, **52**:1647–1655.
45. Xiong Z, Laird PW: **COBRA: a sensitive and quantitative DNA methylation assay.** *Nucleic Acids Res* 1997, **25**:2532–2534.
46. Flaveny C, Reen RK, Kusnadi A, Perdew GH: **The mouse and human Ah receptor differ in recognition of LXXLL motifs.** *Arch Biochem Biophys* 2008, **471**:215–223.
47. Kino T, Gragerov A, Kopp JB, Stauber RH, Pavlakis GN, Chrousos GP: **The HIV-1 virion-associated protein Vpr is a coactivator of the human glucocorticoid receptor.** *J Exp Med* 1999, **189**:51–62.
48. Fritsche E, Schäfer C, Calles C, Bernsmann T, Bernshausen T, Wurm M: **Lightening up the UV response by identification of the arylhydrocarbon receptor as a cytoplasmic target for ultraviolet B radiation.** *Proc Natl Acad Sci USA* 2007, **104**:8851–8856.
49. Beischlag TV, Luis Morales J, Hollingshead BD, Perdew GH: **The aryl hydrocarbon receptor complex and the control of gene expression.** *Crit Rev Eukaryot Gene Expr* 2008, **18**:207–250.
50. Goodier JL, Mandal PK, Zhang L, Kazazian HH Jr: **Discrete subcellular partitioning of human retrotransposon RNAs despite a common mechanism of genome insertion.** *Hum Mol Genet* 2010, **19**:1712–1725.
51. Doucet AJ, Hulme AE, Sahinovic E, Kulpa DA, Moldovan JB, Kopera HC, Athanikar JN, Hasnaoui M, Bucheton A, Moran JV, Gilbert N: **Characterization of LINE-1 ribonucleoprotein particles.** *PLoS Genet* 2010, **6**:e1001150.
52. Martin SL: **Nucleic acid chaperone properties of ORF1p from the non-LTR retrotransposon, LINE-1.** *RNA Biol* 2010, **7**:706–711.
53. Woodcock DM, Lawler CB, Linsenmeyer ME, Doherty JP, Warren WD: **Asymmetric methylation in the hypermethylated CpG promoter region of the human L1 retrotransposon.** *J Biol Chem* 1997, **272**:7810–7816.
54. Muotri AR, Marchetto MC, Coufal NG, Oefner R, Yeo G, Nakashima K, Gage FH: **L1 retrotransposition in neurons is modulated by MeCP2.** *Nature* 2010, **468**:443–446.
55. Tachiwana H, Shimura M, Nakai-Murakami C, Tokunaga K, Takizawa Y, Sata T, Kurumizaka H, Ishizaka Y: **HIV-1 Vpr induces DNA double-strand breaks.** *Cancer Res* 2006, **66**:627–631.
56. Reiss P, Lange JM, de Ronde A, de Wolf F, Dekker J, Danner SA, Debouck C, Goudsmit J: **Antibody response to viral proteins U (vpu) and R (vpr) in HIV-1-infected individuals.** *J Acquir Immune Defic Syndr* 1990, **3**:115–122.

57. Moon HS, Yang JS: **Role of HIV Vpr as a regulator of apoptosis and an effector on bystander cells.** *Mol Cells* 2006, **21**:7–20.
58. Bruggeman LA, Dikman S, Meng C, Quaggin SE, Coffman TM, Klotman PE: **Nephropathy in human immunodeficiency virus-1 transgenic mice is due to renal transgene expression.** *J Clin Invest* 1997, **100**:84–92.
59. Kopp JB, Smith MW, Nelson GW, Johnson RC, Freedman BI, Bowden DW, Oleksyk T, McKenzie LM, Kajiyama H, Ahuja TS, Berns JS, Briggs W, Cho ME, Dart RA, Kimmel PL, Korbet SM, Michel DM, Mokrzycki MH, Schelling JR, Simon E, Trachtman H, Vlahov D, Winkler CA: **MYH9 is a major-effect risk gene for focal segmental glomerulosclerosis.** *Nat Genet* 2008, **40**:1175–1184.
60. Kao WH, Klag MJ, Meoni LA, Reich D, Berthier-Schaad Y, Li M, Coresh J, Patterson N, Tandon A, Powe NR, Fink NE, Sadler JH, Weir MR, Abboud HE, Adler SG, Divers J, Iyengar SK, Freedman BI, Kimmel PL, Knowler WC, Kohn OF, Kramp K, Leehey DJ, Nicholas SB, Pahl MV, Schelling JR, Sedor JR, Thornley-Brown D, Winkler CA, Smith MW, Parekh RS, Family Investigation of Nephropathy and Diabetes Research Group: **MYH9 is associated with nondiabetic end-stage renal disease in African Americans.** *Nat Genet* 2008, **40**:1185–1192.
61. Genovese G, Friedman DJ, Ross MD, Lecordier L, Uzureau P, Freedman BI, Bowden DW, Langefeld CD, Oleksyk TK, Uscinski Knob AL, Bernhardy AJ, Hicks PJ, Nelson GW, Vanhollebeke B, Winkler CA, Kopp JB, Pays E, Pollak MR: **Association of trypanolytic ApoL1 variants with kidney disease in African Americans.** *Science* 2010, **329**:841–845.
62. Winston JA, Bruggeman LA, Ross MD, Jacobson J, Ross L, D'Agati VD, Klotman PE, Klotman ME: **Nephropathy and establishment of a renal reservoir of HIV type 1 during primary infection.** *N Engl J Med* 2001, **344**:1979–1984.
63. Bruggeman LA, Ross MD, Tanji N, Cara A, Dikman S, Gordon RE, Burns GC, D'Agati VD, Winston JA, Klotman ME, Klotman PE: **Renal epithelium is a previously unrecognized site of HIV-1 infection.** *J Am Soc Nephrol* 2000, **11**:2079–2087.
64. Layton DW, Bogen KT, Knize MG, Hatch FT, Johnson VM, Felton JS: **Cancer risk of heterocyclic amines in cooked foods: an analysis and implications for research.** *Carcinogenesis* 1995, **16**:39–52.
65. Scott KA, Turesky RJ, Wainman BC, Josephy PD: **Hplc/electrospray ionization mass spectrometric analysis of the heterocyclic aromatic amine carcinogen 2-amino-1-methyl-6-phenylimidazo[4,5-b]pyridine in human milk.** *Chem Res Toxicol* 2007, **20**:88–94.
66. Puig O, Caspary F, Rigaut G, Rutz B, Bouveret E, Bragado-Nilsson E, Wilm M, Séraphin B: **The tandem affinity purification (TAP) method: a general procedure of protein complex purification.** *Methods* 2001, **24**:218–229.

doi:10.1186/1742-4690-10-83
Cite this article as: Iijima *et al.*: Viral protein R of human immunodeficiency virus type-1 induces retrotransposition of long interspersed element-1. *Retrovirology* 2013 **10**:83.

PLOS ONE

CD8$^+$ T Cell Cross-Reactivity Profiles and HIV-1 Immune Escape towards an HLA-B35-Restricted Immunodominant Nef Epitope

Chihiro Motozono[1,2], John J. Miles[1,3,4], Zafrul Hasan[2], Hiroyuki Gatanaga[2,5], Stanley C. Meribe[2], David A. Price[1], Shinichi Oka[2,5], Andrew K. Sewell[1*9], Takamasa Ueno[2*9]

1 Institute of Infection and Immunity, Cardiff University School of Medicine, Heath Park, Cardiff, United Kingdom, **2** Center for AIDS Research, Kumamoto University, Kumamoto, Japan, **3** Australian Centre for Vaccine Development, Human Immunity Laboratory, Queensland Institute of Medical Research, Brisbane, Australia, **4** School of Medicine, The University of Queensland, Brisbane, Australia, **5** AIDS Clinical Center, National Center for Global Health and Medicine, Tokyo, Japan

Abstract

Antigen cross-reactivity is an inbuilt feature of the T cell compartment. However, little is known about the flexibility of T cell recognition in the context of genetically variable pathogens such as HIV-1. In this study, we used a combinatorial library containing 24 billion octamer peptides to characterize the cross-reactivity profiles of CD8$^+$ T cells specific for the immunodominant HIV-1 subtype B Nef epitope VY8 (VPLRPMTY) presented by HLA-B*35:01. In conjunction, we examined naturally occurring antigenic variations within the VY8 epitope. Sequence analysis of plasma viral RNA isolated from 336 HIV-1-infected individuals revealed variability at position (P) 3 and P8 of VY8; Phe at P8, but not Val at P3, was identified as an HLA-B*35:01-associated polymorphism. VY8-specific T cells generated from several different HIV-1-infected patients showed unique and clonotype-dependent cross-reactivity footprints. Nonetheless, all T cells recognized both the index Leu and mutant Val at P3 equally well. In contrast, competitive titration assays revealed that the Tyr to Phe substitution at P8 reduced T cell recognition by 50–130 fold despite intact peptide binding to HLA-B*35:01. These findings explain the preferential selection of Phe at the C-terminus of VY8 in *HLA-B*35:01*$^+$ individuals and demonstrate that HIV-1 can exploit the limitations of T cell recognition *in vivo*.

Citation: Motozono C, Miles JJ, Hasan Z, Gatanaga H, Meribe SC, et al. (2013) CD8$^+$ T Cell Cross-Reactivity Profiles and HIV-1 Immune Escape towards an HLA-B35-Restricted Immunodominant Nef Epitope. PLoS ONE 8(6): e66152. doi:10.1371/journal.pone.0066152

Editor: Paul A. Goepfert, University of Alabama, United States of America

Received January 10, 2013; **Accepted** May 1, 2013; **Published** June 17, 2013

Funding: This research was supported by a grant-in-aid for scientific research and a Global COE Program (Global Education and Research Center Aiming at the Control of AIDS) from the Ministry of Education, Science, Sports, and Culture (MEXT), and by a grant-in-aid for AIDS research from the Ministry of Health, Labor, and Welfare of Japan (to TU). ZH and SCM are supported by scholarships from The International Priority Graduate Programs, MEXT. JJM is a National Health and Medical Research Council (NHMRC) Career Development Fellow. The authors' studies of TCR binding degeneracy were made possible by generous support from the Biotechnology and Biological Sciences Research Council (grant BB/H001085/1 to AKS and DAP). The funders had no role in study design, data collection and analysis, decision to publish, or preparation of the manuscript.

Competing Interests: The authors have declared that no competing interests exist.

* E-mail: uenotaka@kumamoto-u.ac.jp (TU); sewellak@cardiff.ac.uk (AKS)

9 These authors contributed equally to this work.

Introduction

Hypervariable viruses such as HIV-1 can escape from human leukocyte antigen class I (HLA-I)-restricted CD8$^+$ T cell responses by acquiring viral genomic mutations within or near immunogenic epitopes. Such immune escape pathways can be extremely reproducible and broadly predictable based on host HLA-I alleles at a population level [1,2]. Somewhat paradoxically, however, antigen cross-reactivity is an inbuilt feature of the T cell compartment [3,4]. Indeed, a single autoimmune T cell receptor (TCR) has recently been shown to recognize more than a million different peptides within a broad cross-reactivity profile encompassing unrelated amino acid substitutions [5]. Furthermore, several lines of evidence suggest that certain CD8$^+$ T cell subsets with the capacity to cross-recognize naturally occurring viral variants are advantageous for viral control *in vivo* [6–11]. However, the true extent of HIV-1-specific T cell cross-reactivity remains elusive. In the present study, we characterized the cross-reactivity footprints of HIV-1-specific CD8$^+$ T cells using combinatorial peptide library (CPL) scanning to cover all possible amino acid variations at each position of an octamer epitope. Additionally, we analyzed antigenic variation within the targeted epitope region of HIV-1 subtype B. Our investigations focused on CD8$^+$ T cell responses specific for the immunodominant HIV-1 Nef epitope VY8 (VPLRPMTY) presented by HLA-B*35:01 [12,13].

Materials and Methods

Ethics Statement

All study participants provided informed, written consent at the AIDS Clinical Center, National Center for Global Health and Medicine, Japan. The study was approved by the Institutional Review Board of Kumamoto University and National Center for Global Health and Medicine.

Sequence Analysis of Autologous HIV-1

Treatment-naïve individuals (n = 336) with chronic HIV-1 infection (>90% subtype B) attending the AIDS Clinical Center (International Medical Center of Japan) were enrolled for autologous HIV-1 sequence analysis. The median [IQR] plasma viral load was 95,000 [31,000–350,000] copies/ml; the median

Table 1. TCR β composition of $CD8^+$ T cell lines.

Patient	β chain			
	V gene	J gene	CDR3 sequence	Frequency
Pt-100	BV2*01	BJ2-7*01	CASSGEGNYEQYF	1/31
			CASTTDRVYEQYF	1/31
	BV3-1*01	BJ2-5*01	CASSTSSVTETQYF	2/31
		BJ2-7*01	CASSQDIAGVHEQYF	1/31
	BV4-1*01	BJ2-1*01	CASSQTSGSYNEQFF	1/31
	BV6-1*01	BJ1-5*01	CASSEASGIYEQYF	1/31
		BJ2-7*01	CASSEASGIYEQYF	1/31
	BV10-1*01	BJ2-1*01	CASSAAGVEYNEQFF	1/31
	BV11-2*01	BJ1-1*01	CASSFDIVNTEAFF	1/31
		BJ2-1*01	CASSPDLVDNEQFF	4/31
		BJ2-5*01	CASSGAWTGGGETQYF	2/31
		BJ2-7*01	CASSLDLVSYEQYF	1/31
			CASSLGIGRAYEQYF	1/31
	BV12-3*01	BJ1-4*01	CASSLRFATNEKLFF	1/31
	BV27*01	BJ2-5*01	CASSFDTNQETQYF	1/31
		BJ2-7*01	CASSLDTNGYEQYF	1/31
			CASSFQLAGVHGQYF	1/31
			CASSPRLDDEQYF	2/31
			CASSLDTSGYEQYF	2/31
			CASSSDREDSHEQYF	2/31
	BV28*01	BJ2-2*01	CASSSTDRAIPNTGELFF	1/31
		BJ2-3*01	CASSLPGLDSTDTQYF	1/31
		BJ2-7*01	CASSEGQGRYEQYF	1/31
Pt-168	BV2*01	BJ2-7*01	CASSESLAGGPYEQYF	7/31
	BV3-1*01	BJ2-3*01	CASSQEGADTQYF	2/31
	BV3-1*02	BJ2-3*01	CASSQEGAGTQYF	1/31
	BV6-2*01	BJ1-1*01	CASSGGRTDENTEAFF	1/31
		BJ2-1*01	CASSYEREDSGNEQFF	1/31
	BV11-2*01	BJ2-7*01	CASSLDVAGSYEQYF	1/31
			CASSLDIVSYEQYF	1/31
	BV11-3*03	BJ2-3*01	CASSLVLGTGTDTQYF	1/31
	BV12-3*01	BJ2-3*01	CASSWDSISTDTQYF	1/31
		BJ2-7*01	CASSSDGYEQYF	3/31
	BV12-5*01	BJ2-2*01	CASGLAMVVSGELFF	1/31
	BV15*02	BJ2-1*01	CATSRDLVEDEQFF	2/31
	BV20-1*05	BJ2-2*01	CSARDPRTDRGNTGELFF	1/31
	BV24-1*01	BJ2-3*01	CATSVRDDLTGNGPDTQYF	2/31
	BV27*01	BJ2-3*01	CASSLDLRPDTQYF	1/31
	BV28*01	BJ2-5*01	CASSLLGEETRETQYF	4/31
	BV30*01	BJ2-5*01	CAWHTVRVQETQYF	1/31

doi:10.1371/journal.pone.0066152.t001

[IQR] $CD4^+$ T cell count was 242 [64.5–367.5] cells/mm^3. We determined autologous *nef* sequences from plasma viral RNA using a previously reported direct sequencing method [13].

Table 2. TCR β composition of $CD8^+$ T cell clones.

Patient	Clone	β chain		
		V gene	J gene	CDR3 sequence
Pt-19	19-136	BV7-2*03	BJ2-1*01	CASSPTPQGDYEQFF
	19-139	BV11-2*01	BJ1-1*01	CASSLDLVSTEAFF
Pt-33	33-S1	BV4-2*01	BJ2-3*01	CASSQAADAAITDADTQYF
Pt-100	100-K51	BV27*01	BJ2-5*01	CASSFDTNQETQYF
	100-K105	BV11-2*01	BJ1-1*01	CASSFDIVNTEAFF
	100-K810	BV27*01	BJ2-7*01	CASSFQLAGVHGQYF

doi:10.1371/journal.pone.0066152.t002

Generation and Maintenance of $CD8^+$ T cell Lines and Clones

The $CD8^+$ T cell clones (19–136, 19–139 and 33-S1) were established previously [13]. Additional $CD8^+$ T cell lines and clones were generated by VY8 peptide stimulation of peripheral blood mononuclear cells (PBMCs) isolated from *HLA-B*35:01*$^+$ individuals with chronic HIV-1 infection (Pt-100 and Pt-168) with 10 nM of VY8 (VPLRPMTY) peptide. The Institutional Review Board of the National Center for Global Health and Medicine approved both taking samples and generating cell lines, and patients provided the written informed consent. All $CD8^+$ T cell lines and clones were maintained in RPMI 1640 supplemented with 10% fetal calf serum, 10 IU recombinant human interleukin (IL)-2, antibiotics and L-glutamine.

Analysis of TCR-encoding Genes

TCR-encoding genes of $CD8^+$ T cell lines and clones were obtained by using a SMART PCR cDNA synthesis kit (Clontech) and analyzed with reference to the ImMunoGeneTics database (http://imgt.cines.fr) as described previously [14].

T cell Sensitivity Assay

Secretion of cytokines and chemokines by virus-specific $CD8^+$ T cells in response to specific antigen provides a useful tool for quantitative assessment of antigen recognition [15,16]. MIP-1β was used as a functional readout in this study since it is one of the most sensitive means to assess functional avidity of human $CD8^+$ T cells as previously described [15–17]. Briefly, 3×10^4 T cells were mixed with 6×10^4 HLA-B*35:01-expressing C1R cells (C1R-B3501), either unpulsed or pulsed with cognate peptide across a range of concentrations. After overnight incubation at 37°C, the supernatant was harvested and assayed for MIP-1β content by ELISA as described previously [5,17]. The amount of MIP-1β released in the absence of the peptide was subtracted as background. It should be noted that the VY8 peptide titration experiments of T cell clones 136 and 139 exhibited comparable results when IFN-γ [13] and MIP-1β were used as readouts (data not shown).

Figure 1. Amino acid residues preferentially recognized by VY8-specific CD8$^+$ T cells. Graphical representation showing relative preference for amino acid residues recognized by VY8-specific T cell lines and clones based on the CPL scan data shown in Figure S1. Responses >20% were included. A web-based application, WebLogo 3 (http://weblogo.threeplusone.com/), was used to generate the graphic. Colours represent physicochemical properties: polar (G, S, T, Y and C), green; neutral (Q and N), purple; basic (K, R and H), blue; acidic (D and E), red; hydrophobic (A, V, L, I, P, W, F and M), black. The index residues at each position are outlined in yellow. Residue size is proportional to T cell recognition preference.
doi:10.1371/journal.pone.0066152.g001

Octamer Combinatorial Peptide Library (CPL) Scan

The octamer CPL contained a total of 2.4×10^{10} different peptides (PepScan) divided into 160 sub-mixtures in positional scanning format as described previously [4,18]. Target C1R-B3501 cells (6×10^4 cells/well) were pre-incubated in the absence or presence of CPL sub-mixtures (100 μg/ml). Effector T cells (3 x 10^4 cells/well) were then added and incubated overnight at 37°C. Supernatant was collected and analyzed for MIP-1β content by ELISA as described previously [5,17]. Background-subtracted results were expressed as % response, normalized with respect to the VY8 index residue. A response >20% was considered positive.

Results and Discussion

Clonotypic Characterization of VY8-specific T cells

CD8$^+$ T cell lines were established from two *HLA-B*35:01*$^+$ individuals with chronic HIV-1 infection (Pt-100 and Pt-168). Analysis of TCR β usage by these T cell lines revealed multiple clonotypes, with 23 and 17 distinct TCR β sequences for Pt-100 and Pt-168, respectively (Table 1). This observation is consistent with previous studies showing the oligoclonal nature of immunodominant HIV-1-specific CD8$^+$ T cell populations [19,20]. The CD8$^+$ T cell clones K51, K105 and K810 were generated from patient Pt-100 by limiting dilution of VY8-specific T cell lines. Monoclonality was confirmed by TCR β analysis and all three sequences were encompassed within the TCR repertoire of the parental T cell lines (Table 2). Additional CD8$^+$ T cell clones (136, 139, and S1) previously established from two separate *HLA-B*35:01*$^+$ HIV-1-infected individuals [12,13] showed distinct TCR β chain usage (Table 2) and were also used for cross-reactivity studies.

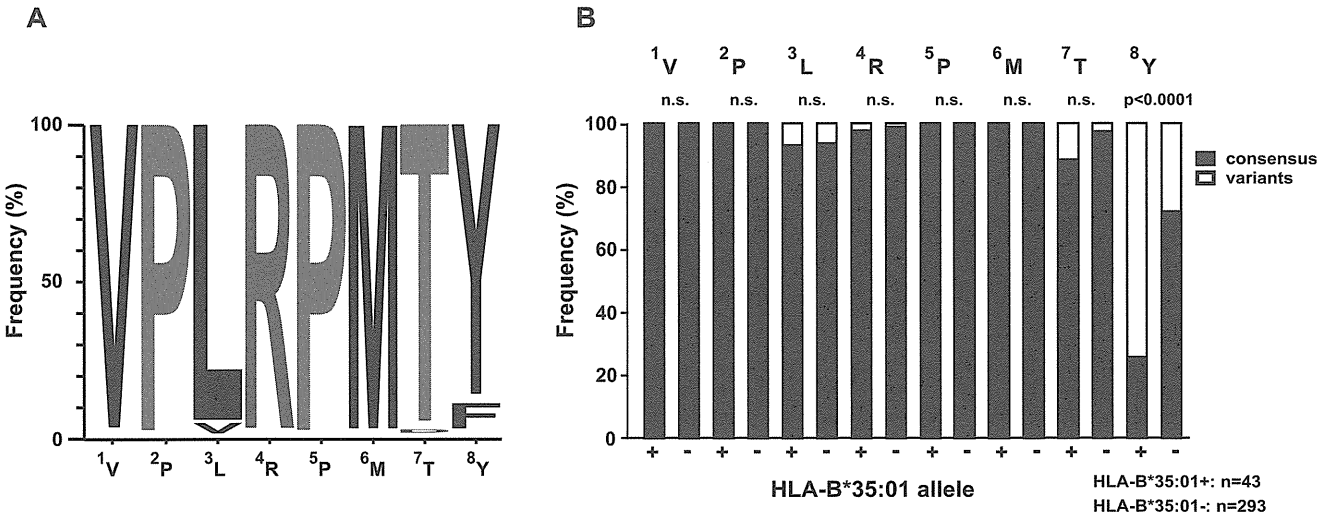

Figure 2. Naturally arising antigenic variations in the VY8 epitope. (**A**) Graphical representation showing the frequency of amino acid residues within the VY8 epitope in subtype B Nef sequences retrieved from the Los Alamos database (n = 1191). WebLogo 3 was used to generate the graphic. (**B**) The frequency of consensus (subtype B) and variant amino acid residues at each position of the VY8 epitope is shown for autologous plasma viral sequences derived from a total of 336 HIV-1-infected individuals, segregated according to *HLA-B*35:01* status. Statistical analysis was performed using Fisher's exact test. *n.s.*, not significant.
doi:10.1371/journal.pone.0066152.g002

Cross-reactivity Analysis of VY8-specific T cells

The cross-reactivity profiles of VY8-specific T cell lines and clones were analyzed using a CPL containing a total of 2.4×10^{10} different octamer peptides, which allowed qualitative mapping of preferred T cell recognition residues at each position along the peptide backbone [4,18]. Different VY8-specific T cell lines and clones preferentially recognized different amino acid residues across the octamer peptide backbone (Figure S1). We employed a graphical representation of these preferential recognition residues by the VY8-specific T cells (Figure 1). Despite these unique cross-reactivity patterns, all T cells tested recognized the index VY8 residues efficiently (Figure 1). This finding contrasts with previous observations using tumor-specific and autoreactive T cell clones [5,21–23], which typically prefer non-index amino acid residues. Across all clones, more stringent recognition was observed at position 2 (P2) and P8 (Figure 1). This most likely reflects the anchor role of these positions in peptide binding to HLA-B*35:01 [12,24]. The VY8-specific T cell clones, K51, K105 and K810, showed inherently unique cross-reactivity footprints but less flexible cross-recognition compared to the parental T cell line (Figure 1), suggesting increased coverage of viral antigenic variation through polyclonal TCR cross-reactivity.

Naturally Occurring Antigenic variations within the VY8 Epitope

To investigate the correlation between T cell cross-reactivity and naturally occurring antigenic variation, we analyzed sequence polymorphisms within the VY8 epitope. Despite the remarkable variability of HIV-1 Nef, VY8 is highly conserved, most likely due to its location partially within a Src homology 3 binding motif that

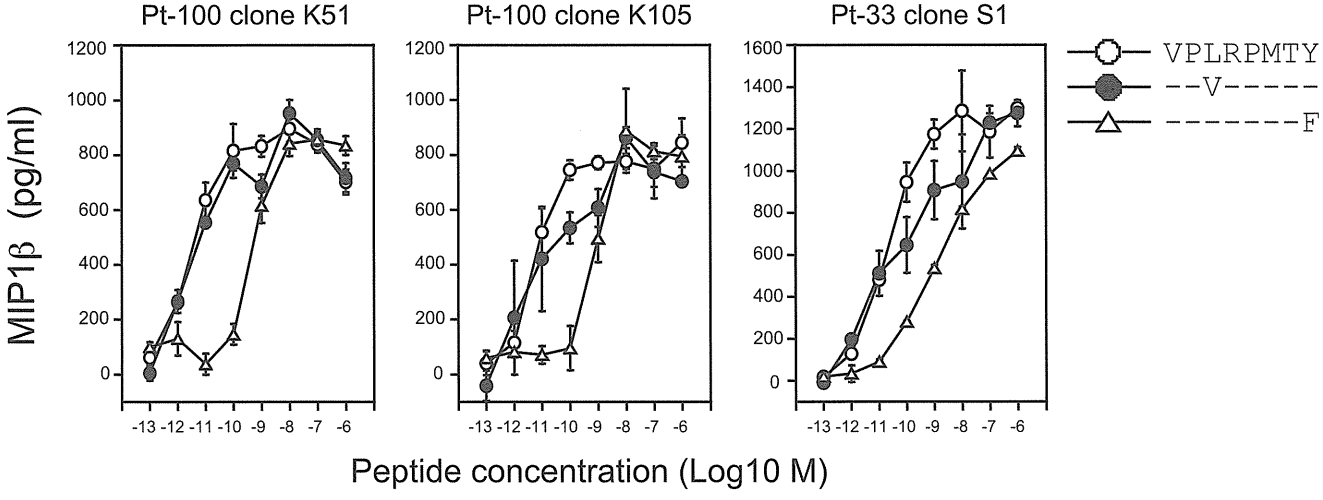

Figure 3. VY8-specific CD8$^+$ T cell sensitivity towards peptide variants. The sensitivity of T cell clones towards the VY8, VY8-3V and VY8-8F peptides was quantified by measuring the amount of MIP-1β secreted in response to antigen stimulation. Data are representative of duplicate assays and standard deviation from the mean of two replicates is shown.
doi:10.1371/journal.pone.0066152.g003

Table 3. Sensitivity of VY8-specific $CD8^+$ T cells.

$CD8^+$ T cells		EC_{50} (M)		
		VY8	VY8-3V	VY8-8F
lines	Pt-100	5.9×10^{-12} (x 1)	nd	3.9×10^{-10} (x 66)
	Pt-168	4.0×10^{-12} (x 1)	nd	4.3×10^{-10} (x 105)
clones	33-S1	2.3×10^{-11} (x 1)	3.9×10^{-12} (x 0.17)	1.2×10^{-9} (x 52)
	100-K51	3.1×10^{-12} (x 1)	5.8×10^{-12} (x 1.8)	4.2×10^{-10} (x 135)
	100-K105	5.1×10^{-12} (x 1)	3.9×10^{-12} (x 0.76)	6.7×10^{-10} (x 131)

EC_{50}, determined by duplicate assays; nd, not done; in parenthesis, fold changes in sensitivity relative to index.
doi:10.1371/journal.pone.0066152.t003

is critical for several Nef functions [25], including HLA-I down-regulation [13,26]. Nevertheless, in the Los Alamos HIV Sequence database (http://www.hiv.lanl.gov/content/index), some variability within HIV-1 subtype B has been reported at P3 Leu and P8 Tyr of the VY8 epitope, with 2.4% and 8.2% of viral clones showing polymorphisms in these positions, respectively (Figure 2A). Given that approximately 40% of Nef sequence polymorphisms are associated with host HLA-I alleles [1], we examined these particular variants for HLA-I association. Our previous smaller study of 69 HIV-1-infected patients indicated that Phe at P8 might be associated with the *HLA-B*35:01* allele [13]. To confirm this association and examine polymorphisms at P3, we recruited a larger cohort comprising 336 treatment-naïve individuals with chronic HIV-1 infection and determined autologous *nef* sequences from plasma viral RNA. Although we found some variability at P3 (3%), there were no statistically significant amino acid differences at P1–P7 between individuals with or without *HLA-B*35:01* (Figure 2B). In fact, CPL scanning showed that, at P3, hydrophobic residues including both the index Leu and mutant Val were preferentially recognized by all VY8-specific T cells tested (Figure 1). Such flexible TCR recognition at P3 helps to explain why the Val mutant is not selected in *HLA-B*35:01*$^+$ individuals. Conversely, we found a statistically significant difference in the frequency of polymorphisms at P8 between individuals with or without *HLA-B*35:01* (Figure 2B); indeed, the vast majority (74%) of *HLA-B*35:01*$^+$ donors harboured viral sequences with Phe at P8. However, CPL scanning showed that Phe was a favoured amino acid residue recognized by T cell lines and some clones, such as K105 (Figure 1 and Figure S1). In these instances, CPL data alone do not simply explain the emergence of this viral mutation in *HLA-B*35:01*$^+$ individuals.

VY8-specific T cell Sensitivity Towards Peptide Variants

To verify the effect of single mutations within the VY8 peptide on TCR sensitivity, we performed competitive titration assays across our panel of VY8-specific T cells (Figure 3). Consistent with the CPL scan data, all T cells tested recognized the VY8 and VY8-3V peptides comparably (<2 fold difference in EC_{50} values; Table 3). In contrast, the EC_{50} values for VY8-8F were >50 fold higher than index for all T cells tested (Table 3). These observations are consistent with previous reports showing that VY8-specific T cells could not recognize $CD4^+$ T cells or macrophages infected with HIV-1 carrying this Nef variant at P8 [13,26].

Although P8 is an anchor residue for VY8, our previous HLA-I stabilization studies showed comparable binding activity between HLA-B*35:01 and either VY8 or VY8-8F [13]. The crystal structure of the VY8/HLA-B*35:01 complex shows that P8 Tyr lies deep inside the F pocket of the HLA-I molecule [24]. Substitution at this position with the aromatic residue Phe may not induce substantial structural changes. Consequently, impaired T cell recognition of P8 Phe may be mediated by indirect conformational changes imposed by the peptide upon TCR binding [17]. In the context of HLA-A*02:01, however, a Tyr to Phe substitution at the secondary anchor P3 of an antigenic peptide (SLFNTVATL) leads to unexpectedly large conformational changes in the peptide backbone [27]. Accordingly, further structural studies are needed to elucidate the precise mechanism through which anchor residue substitution leads to impaired T cell recognition of the VY8 epitope.

Previous studies have shown that the double substitution of Arg-71 to Thr and Tyr-81 to Phe (P8 at VY8) [13], or Pro-75 to Ala (P2 at VY8) as a single mutation, impair Nef-mediated down-regulation of HLA-I and thereby increase the susceptibility of HIV-1-infected cells to killing by $CD8^+$ T cells targeting other epitopes [26,28]. In contrast, the Tyr-81 to Phe (P8 at VY8) mutation alone exerts virtually no effect on Nef-mediated activities [13,26]. Collectively, these data suggest that the P8 Phe mutation does not compromise viral fitness.

Concluding Remarks

$CD8^+$ T cell responses against the immunominant HIV-1 subtype B-derived Nef epitope VY8 presented by HLA-B*35:01 are highly polyclonal, broadly cross-reactive and capable of tolerating natural viral variation with one notable exception. Specifically, the observed Phe substitution at P8, which is neutral in terms of Nef-mediated function [13,26], was found to reduce $CD8^+$ T cell recognition by >50 fold. The association of this mutation with *HLA-B*35:01*$^+$ strongly suggests that evasion of VY8-specific $CD8^+$ T cell activity confers a selection advantage *in vivo*. Thus, even $CD8^+$ T cell responses with extensive cross-reactivity profiles can succumb to immune escape at a single position.

Supporting Information

Figure S1 CPL scanning of VY8-specific $CD8^+$ T cells. The cross-reactivity profiles of T cell lines and clones specific for VY8 were tested by using 160 CPL sub-mixtures (100 μg/ml) comprising a total of 2.4×10^{10} different octamer peptides. In every peptide mixture, one position has a fixed amino acid residue and all other positions are degenerate, with the possibility of any one of 19 natural amino acids being incorporated in each individual position (cysteine is excluded). The amount of MIP-1β secreted in response to antigen was quantified by ELISA. Data are background-subtracted and the relative T cell response is shown as a ratio of MIP-1β production with respect to the index residue at each position. Responses >20% were considered positive and used to construct Figure 1. A representative set of duplicate assays is shown. Red bars depict residues corresponding to the VY8 index sequence.
(EPS)

Acknowledgments

We thank Dr. L. Wooldridge for providing reagents and assistance for this study.

Author Contributions

Conceived and designed the experiments: CM JJM AKS TU. Performed the experiments: CM JJM ZH SCM TU. Analyzed the data: CM JJM ZH